Research Square

Preprints are preliminary reports that have not undergone peer review.
They should not be considered conclusive, used to inform clinical practice,
or referenced by the media as validated information.

Development of a Novel Rule-Based Controlled Strategy on a Hybrid Electric UAV

Lionel Fouellefack
University of South Africa
Etienne Feukeu
efeukeea@unisa.ac.za
University of South Africa
Sumbwanyambe Mbuyu
University of South Africa
Dhlamini Mokhotjwa
University of South Africa

Research Article

Keywords: Unmanned Aerial Vehicles, Hybrid Electric Propulsion Systems (HEPS), Energy Management Strategy, Internal Combustion Engine (ICE), Electric Motor (EM)

Posted Date: June 19th, 2026

DOI: https://doi.org/10.21203/rs.3.rs-10008531/v1

License: This work is licensed under a Creative Commons Attribution 4.0 International License.
Read Full License

Additional Declarations: No competing interests reported.

Development of a Novel Rule-Based Controlled Strategy on a Hybrid Electric UAV

Lionel Fouellefack[1], Etienne Alain Feukeu [2] Sumbwanyambe Mbuyu[3] and Dhlamini Mokhotjwa [4]

1 Department of Electrical and Smart Systems Engineering, University of South Africa, Pretoria, South Africa
* Correspondence: 25201662@mylife.unisa.ac.za s

Abstract:

Hybrid electric propulsion has gained significant attention in reducing the fuel consumption and pollution emissions of Unmanned Aerial Vehicles (UAVs). The problem of managing the energy within the powertrain of the aircraft is still a major concern within the aviation industry. This can be accomplished through an effective energy management strategy that ensures that the energy within the aircraft is properly distributed. In this paper, a novel rule-based control strategy is developed as an energy management strategy for a fixed-wing UAV used for intelligence surveillance and reconnaissance (ISR) missions. Firstly, a simulation model of four powertrain architectures of the aircraft is presented: Conventional, electric, serial hybrid, and parallel hybrid architectures. Then, a novel rule-based control strategy was developed as an energy management strategy, allowing the aircraft to switch between various operating modes throughout its mission. Through simulation, it was shown that the aircraft with hybrid electric propulsion systems could save about 22% of fuel compared to an aircraft with a conventional powertrain system for varying mission profiles.

Keywords: Unmanned Aerial Vehicles; Hybrid Electric Propulsion Systems (HEPS); Energy Management Strategy; Internal Combustion Engine (ICE), Electric Motor (EM)

1 Introduction

The Electric-powered UAVs cannot achieve high range and endurance due to the limitations in their battery-specific energy density. Internal Combustion Engine (ICE) - powered UAVs or conventional architectures can achieve higher range and endurance than their electric counterparts, but they produce a lot of noise and thermal signatures, which is undesirable, especially if the UAV has to patrol in the air for very long distances [1][2][3]. Also, UAVs with conventional architectures produce a lot of harmful emissions, which pollute the atmosphere, contributing to global warming [4][5]. A report from National Geographic shows that aviation alone produces about 12% of total CO2 emissions [6], with about 700 million tons emitted by aircraft in 2013[6]. Additionally, with the shortages of fossil fuels, there is a need for engineers to develop alternative powertrain architectures for UAVs that will satisfy the range and endurance requirements of the aircraft while meeting the stringent requirements of fuel consumption and atmospheric emissions. Hybrid propulsion technology has become a promising solution for engineers and scientists to increase the UAV endurance and range, as it utilizes two or more power sources that can be used interchangeably during flight. Many Universities and aerospace companies are actively researching this hybrid technology approach by developing hybrid powertrain architectures that use more than two power sources, which could be batteries, fossil fuels, fuel cells, or photovoltaic cells, to increase the UAV range. A 13.6kg Fixed-Wing airplane with a hybrid-electric propulsion system has been built by students from the Air Force Institute of Technology to improve the endurance of their ICE – powered UAV [7]. A group of Aerospace

Engineering students from the University of Colorado, the University of Stuttgart, and the University of Sydney associated together to develop a UAV using hybrid propulsion technology (Hyperion UAV)[8]. The University of Sydney researchers built a hybrid electric UAV (SUAV) and Grob 109 UAV using fuel cells and batteries to evaluate the endurance of the UAV for given mission Profiles [9][10]. Also, a 13.4kg hybrid-electric UAV using fuel cells and batteries was built by researchers from Cranfield University [11]. Aerospace companies such as Quatermium [12], AeroVironment [13], and Lockheed Martin [14] are also developing UAVs using hybrid Technology to improve the endurance of electric-powered UAVs. Four main variants of powertrain architectures for aircraft exist, which are classified according to literature into Electric Architecture, Series Hybrid Architecture, Parallel Hybrid Architecture, and Series-Parallel Hybrid Architecture [1][15][16]. In the electric architecture, energy is supplied by the battery to drive the propulsion system [17]. With this powertrain configuration, the UAV can only achieve a limited endurance due to the limited specific energy density of its battery [18]. In the series hybrid architecture, the energy that drives the propulsor of the UAV comes from the electric motor [1]. In the parallel hybrid architecture, energy is supplied to the propulsion by the ICE and electric motor, which comes from at least two energy sources (ie, Fuel and Battery), which drives the propeller of the aircraft either simultaneously or individually [1]. The series-parallel architecture is not widely employed on UAVs due to its bulky nature. Since the main aim of the paper is to do a comparative study in terms of range endurance and fuel consumption achieved by each architecture type of the aircraft, only the electric, series hybrid, and parallel hybrid architectures were considered for investigation. The three powertrain architectures are shown in Figure 1, Figure 2, and Figure 3, respectively.

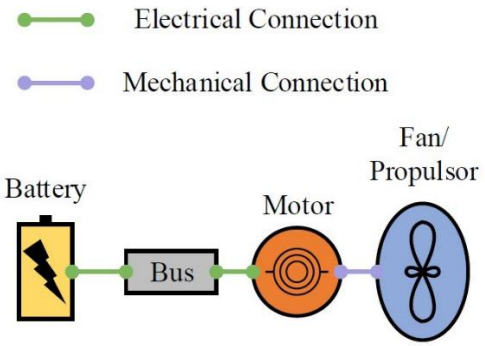


Figure 1: All – Electric Powertrain Architecture [17]

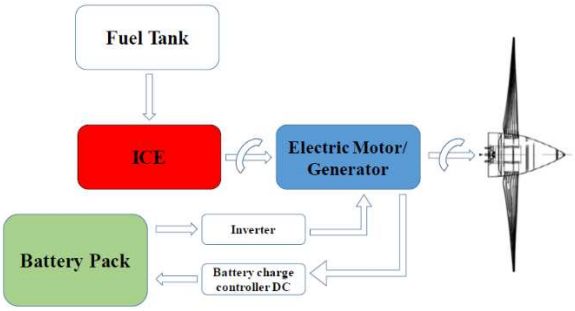


Figure 2: Series Hybrid Powertrain Architecture [19]

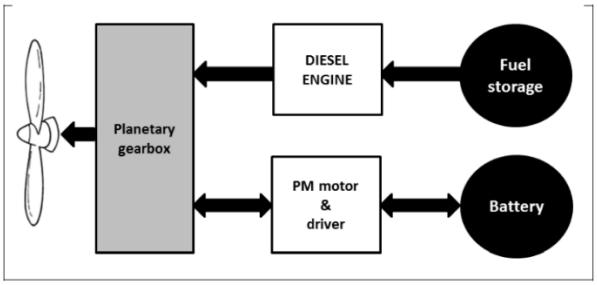


Figure 3: Parallel Hybrid Powertrain Architecture [20]

A supervisory controller ensures that energy is properly distributed within the powertrain of an aircraft. They are broadly classified into rule-based [21][22] and optimization-based strategies [23]. In this paper, a rule-based controlled strategy was investigated as an energy management strategy (EMS) as it allows the UAV to switch between various operating modes using some controlled decisions to improve the fuel consumption of the aircraft. Previous researchers have used this controlled strategy as an energy management strategy on an aircraft. The contribution of each author's work and limitations identified are discussed below: C He. Et al (2020) [24] employed this control method to characterize the split of the power demand during different flight phases of the tilt-wing UAV (Vertical flight mode, transition mode, and forward flight mode) during different mission phases of the UAV. The author did not, however, employ the control strategy to optimize other parameters of the aircraft, such as fuel consumption and payload mass. Donate et al. (2017) [25] used a rule-based EMS to characterize the split between the power sources of a parallel hybrid electric power system (HEPS) consisting of a two-stroke diesel engine and electric machine in five operating modes: hybrid Mode, motor mode, engine mode, charging mode, and electric mode. Using the method, the author was able to achieve a fuel reduction of 12% and 8% compared to the non–hybrid case when the battery was sized for 30 minutes and 60 minutes in electric flight, respectively. Hung, J. (2012) [26] developed a rule-based controlled strategy to minimize the fuel consumption of a UAV using a parallel HEPS. The controller allows the UAV to switch between different operational modes (Hybrid Climbing, Engine only, Hybrid Charging, Hybrid Normal mode, Motor only mode) during the mission of the aircraft. The UAV achieved a 6.5% fuel savings using this configuration compared to the engine-only configuration. The work, however, did not consider other rule-based control schemes to obtain better fuel savings, with the limited fuel savings achieved. Wang et al (2019) [27] developed a rule-based controlled EMS on a UAV utilizing a distributed series HEPS using an engine and electric motor. The rule-based strategy allowed switching between three operating modes (Electric Mode, Ideal Mode, and Max Power mode). The author did not, however, obtain any conclusive results in terms of fuel consumption and payload achieved during a flight mission. Y Xie et al (2018) [28] implemented a rule-based controlled strategy on a UAV utilizing a parallel HEPS to reduce the fuel consumption of the UAV. The controlled strategy developed enabled the UAV to operate in four modes (Electric Mode, Fuel Mode, Charging Mode, and Combined Mode) throughout the UAV's mission. Through simulations, the authors were able to achieve a 7% fuel consumption reduction compared to an ICE-powered aircraft. The author did not, however, consider any optimization strategy to obtain better results with the limited fuel consumption achieved. In addition, other powertrain architectures were not investigated. Suti et al (2021) [29] developed a rule-based controlled strategy for a parallel hybrid-electric UAV to evaluate the feasibility of converting an ICE-based propulsion system into a HEPS. The developed controller allowed the UAV to operate in 3 Modes: Generator Mode/Battery disengaged, Generator Mode/Battery Engaged, and Booster Mode. The author, however, did not achieve any conclusive results regarding fuel consumption, payload capacity, and power required of the UAV

during a full mission with the developed controlled strategy. D Hyun et al (2024) [30] developed a rule-based EMS on a hybrid UAV using battery and fuel power sources for crop spraying missions. J Wilson (2024) [31] developed a hybrid powertrain model framework using rule-based controlled EMS on a UAV using a parallel hybrid powertrain to evaluate its performance on a hybrid power testbench. The controller was operated in three modes: electric mode, combustion engine mode, and hybrid mode. The author did not, however, provide any conclusion regarding the fuel consumption achieved on his developed powertrain model and control strategy employed. C Greiser et al (2011) [32] developed a rule-based controlled strategy for a remotely piloted aircraft with a parallel HEPS, which was tested on a hybrid power test plant built by the authors. The developed controller was tested on the hybrid power test plant in four distinct flight modes (cruise mode, restart mode, endurance mode, and climb mode). The developed controlled strategy from the research did not provide any conclusive results regarding fuel consumption, payload capacity, or energy usage in the developed powertrain system. Also, the work was limited to a parallel hybrid-electric architecture. Boggero et al (2019) [33] presented a simulation model of a virtual test bench of a UAV with a parallel HEPS. The developed model was evaluated in various operating modes over the flight profile of the UAV. The work, however, did not carry out any fuel consumption analysis to evaluate the fuel burn and energy savings during the mission of the UAV. Work was limited to a parallel hybrid architecture, as only a single powertrain architecture was considered. JMT Matlock (2019) [34] developed a simulation model of parallel hybrid electric UAVs using rule-based control EMS. The developed controller was evaluated on a parallel hybrid power test bench constructed by the author to test its operation in 3 modes (ICE Mode, EM mode, and combined mode). The author did not, however, provide any conclusion regarding fuel consumption, energy usage, and payload capacity achieved during the flight mission of the UAV. D Obertino et al (2021) [35] implemented a rule-based controlled strategy and a simulation framework on a UAV with a parallel HEPS. Two controllers were implemented: the Serial Hybrid Controller, which allowed switching between the designed mode with power provided by the electric motor throughout the flight mission of the UAV, and the parallel hybrid controller, which allowed the UAV to switch into four modes: recharge mode, stealth mode, dash mode, and normal mode, throughout the mission of the UAV. The work did not, however, provide any conclusion on the endurance and fuel consumption achieved by each hybrid contribution.

The paper is divided into the following sections: Section 2 presents the modelling and simulation of the drive components for propulsion of the UAV, Section 3, presents the Simulink Models of the different powertrain architectures, Section 4, presents the rule based controlled strategy developed for the serial and parallel powertrain architecture of the UAV, Section 5 presents the results obtained and section 6 gives a summary results of the finding obtained and future directions.

Three main original contributions were achieved in this research:

A simulation model of four powertrain architectures of the aircraft was developed and presented i.e conventional, electric, serial hybrid electric, and parallel hybrid electric architectures.

A simulation model of a UAV with a parallel hybrid electric architecture was presented, which estimates the power, torque, BSFC, and fuel flow of the hybrid electric aircraft for given mission profiles.

A novel rule-based control strategy was implemented on a UAV with a parallel hybrid electric architecture, which allows the UAV to save about 22% fuel consumption compared to the conventional powertrain of the aircraft.

2 Modelling and Simulation

This Methods Various drive components for propulsion of the UAV were modelled in Matlab – Simulink environment: battery, electric motor, generator, combustion engine, propeller, DC – DC converter, Electronic Speed Control, Fuel System, UAV, and clutch.

2.1. Battery Model

The battery model subsystem was implemented using the Shepherd nonlinear circuit modelling approach. Using this modelling approach, the battery voltage, current, and State of Charge (SOC) are modelled at any given time step [36][37]. Figure 4 shows the circuit diagram of the battery.

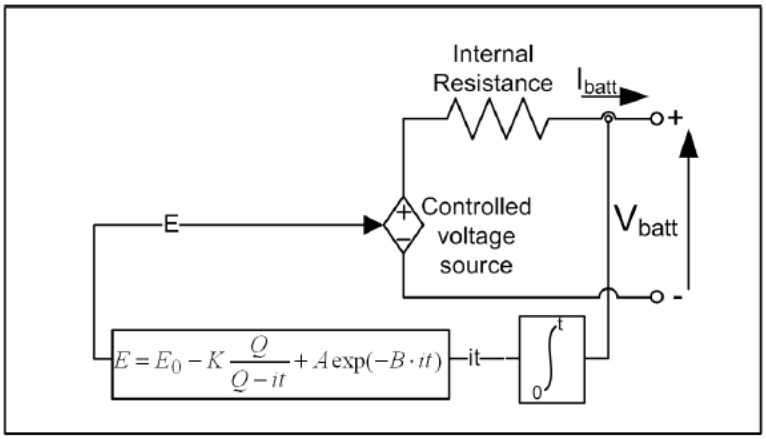


Figure 4: Shepherd's Non–Linear Equivalent

The battery modelling equations are defined in charge and discharge mode as:

Discharge Mode:

$$V_{batt} = E_0 - R_0 i_b - K\frac{Q}{Q - i_b t}.(i_b t + i^*) + Aexp(-Bi_b t) - - - - - - - - - - - (1)$$

$$SOC_f = SOC_0 - \frac{\int_{t_0}^{t} i_b dt}{Q_b} - (2)$$

Charge Mode:

$$V_{batt} = E_0 - R_0 i_b - K\left(\frac{Q}{it - 0.1Q}\right)i^* - K\left(\frac{Q}{Q - it}\right)it + Aexp(-B.i_b t) - - - - - (3)$$

$$SOC_f = SOC_0 + \frac{\int_{t_0}^{t} i_b dt}{Q_b} - (4)$$

Where: V_{batt} is battery voltage (V), E_0 is the battery constant voltage (V), K is the polarization resistance Ω, Q is the battery capacity (Ah), A is the exponential zone amplitude (V), B is the exponential zone time constant inverse $(Ah)^{-1}$ R_0 is the internal resistance (Ω), i_b is the battery current (A), i^* is the filtered current (A). figure 5, figure 6, figure 7 and figure 8 shows simulink models of the developed battery.

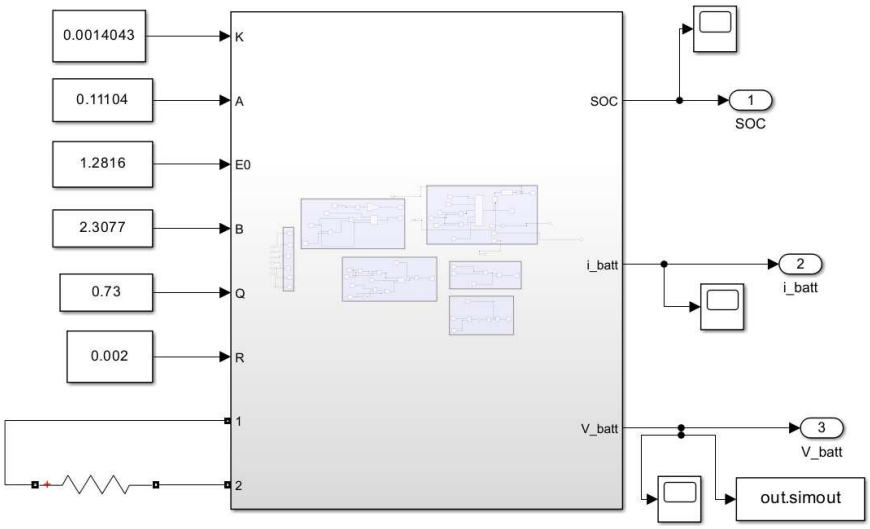


Figure 5: Simulink Model of the Battery

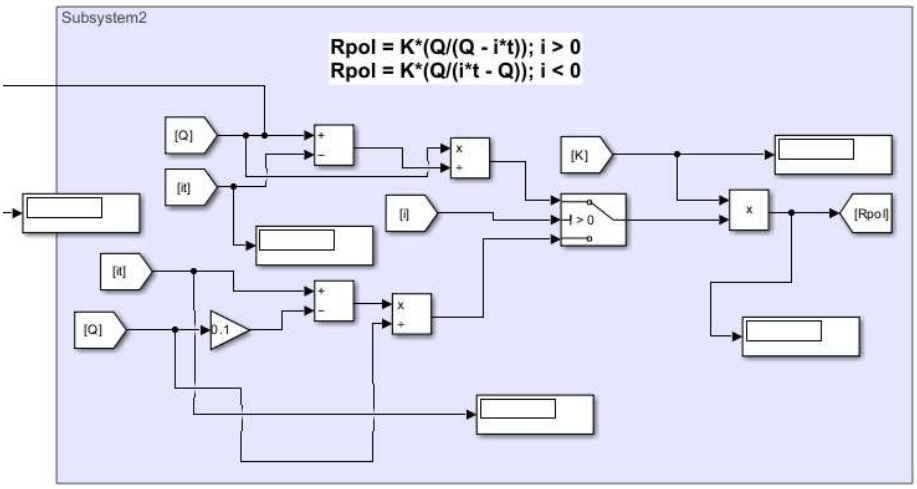


Figure 6: Polarisation Resistance Calculation in Simulink

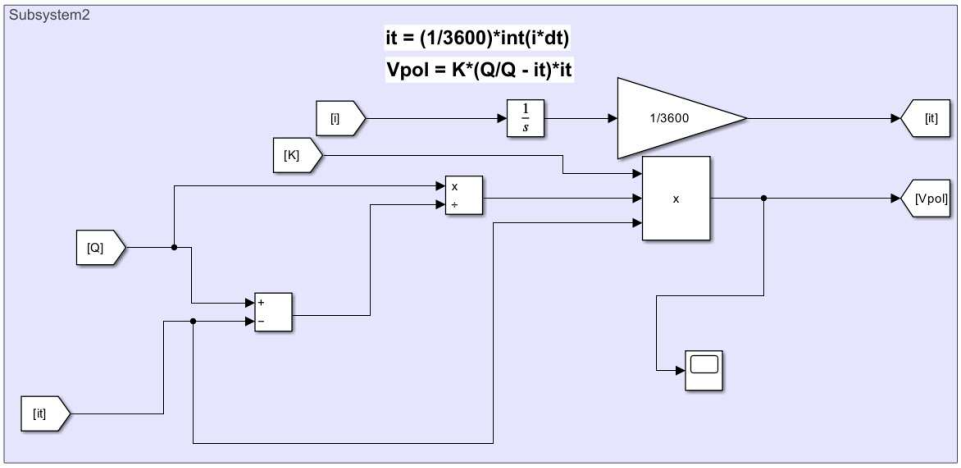


Figure 7: Polarisation Calculation Voltage Calculation in Simulink

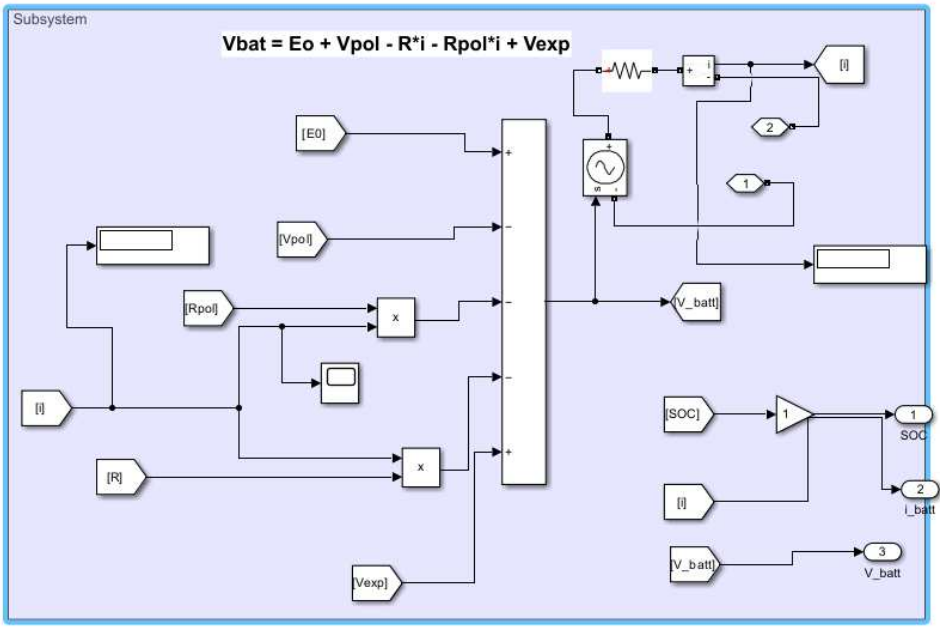


Figure 8: Battery Voltage Calculation in Simulink

The battery model was parametrized using the same input parameters as those obtained from the literature.[38] (k = 0.12, A = 0.55, $E_0 = 13.4$ B = 83, R = 0.3). The results show that the battery model discharge voltage closely matches that obtained experimentally, as shown in Figure 9.

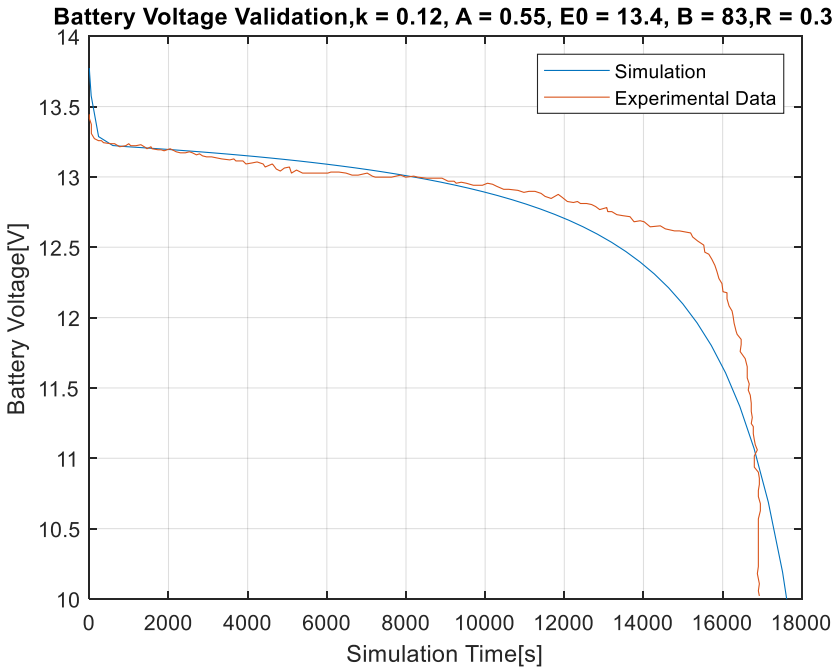


Figure 9: Battery Model Validation With Experimental Data from Manufacturer Data Sheet

2.2. Electric Motor Model

The electric motor was modelled in Simulink using equations of the first-order DC electric motor model by Mark Drela [39]. Figure 10 shows the equivalent circuit model using this modelling approach.

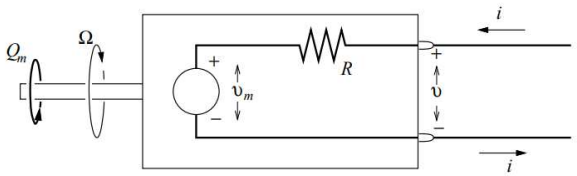


Figure 10: Equivalent Circuit of a DC Electric Motor

The main equations using this modelling approach are defined as:

$$Q_m(i) = \frac{(i - i_0)}{K_Q} - - - - - - - - - - - - - (5)$$

$$v_m(\Omega) = \frac{\Omega}{K_v} - - - - - - - - - - (6)$$

$$v(i, \Omega) = v_m(\Omega) + i\mathcal{R} = \frac{\Omega}{K_v} + i\mathcal{R} - - - - - (7)$$

Where: K_Q is the motor torque constant, i_0 is the no – load current, i is the terminal current, K_v is the motor speed constant, Ω is the motor rotational speed. Figure 11 shows the Simulink model of the electric motor.

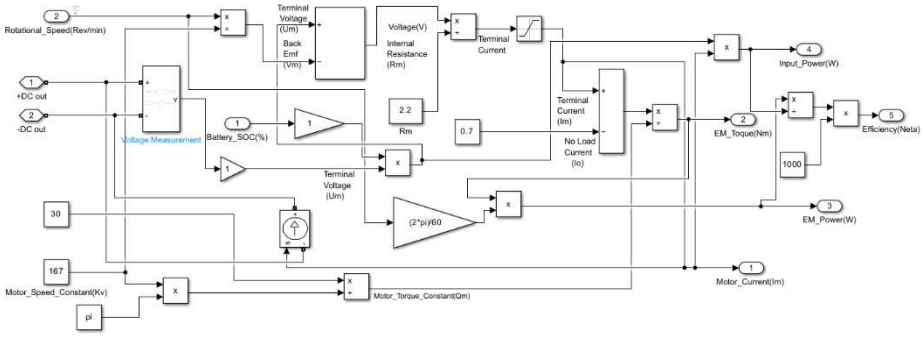


Figure 11: Simulink Model of the Electric Motor

The electric motor back EMF is determined by the model as:

$$v_m(\Omega) = \frac{\Omega}{K_v} \quad (8)$$

The motor terminal current is determined by the model as:

$$i(\Omega, \mathrm{v}) = \frac{v - v_m(\Omega)}{R} \quad (9)$$

Substituting equation (8) into (9) the motor terminal current equation can be rewritten as:

$$i(\Omega, \mathrm{v}) = \left(v - \frac{\Omega}{K_v}\right) * \frac{1}{\mathcal{R}} \quad (10)$$

The motor torque is determined by the model as:

$$Q_m(\Omega, \mathrm{v}) = [i(\Omega, \mathrm{v}) - i_0] * \frac{1}{K_Q} \quad (11)$$

Substituting equation (10) into (11) the motor torque can be rearranged as:

$$Q_m(\Omega, \mathrm{v}) = \left[\left(v - \frac{\Omega}{K_v}\right) * \frac{1}{\mathcal{R}} - i_0\right] * \frac{1}{K_Q}$$

The motor output power is determined by the model as:

$$P_{shaft}(\Omega, \mathrm{v}) = Q_m(\Omega, \mathrm{v}) \times \Omega$$

$$= \left[\left(v - \frac{\Omega}{K_v}\right) * \frac{1}{\mathcal{R}} - i_0\right] * \frac{\Omega}{K_Q}$$

The motor efficiency is determined by the model as:

$$\eta_m(\Omega, \mathrm{v}) = \frac{P_{shaft}(\Omega, \mathrm{v})}{P_{in}}$$

$$= \frac{P_{shaft}(\Omega, \mathrm{v})}{iv}$$

$$= \left(1 - \frac{i_0}{i}\right)\frac{K_v}{K_Q}\frac{1}{1 + i\mathcal{R}\,K_v/\Omega}$$

The derived equations were used to develop the Simulink model of the electric motor. The model was run at various input voltages to obtain the power, torque and current of the electric motor as a function of rotational speed as shown in figure 12, figure 13 and figure 14 respectively.

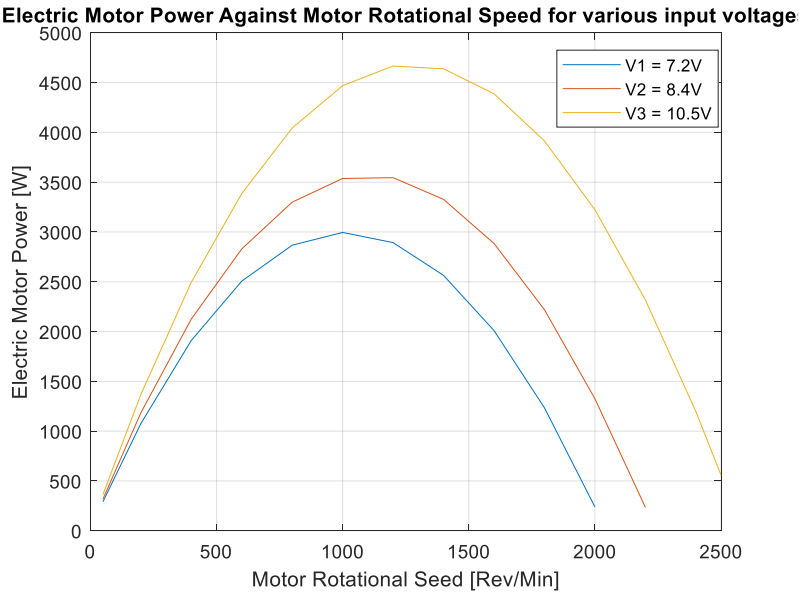


Figure 12: Electric Motor Power Against Motor Rotational Speed at Various Input Voltages

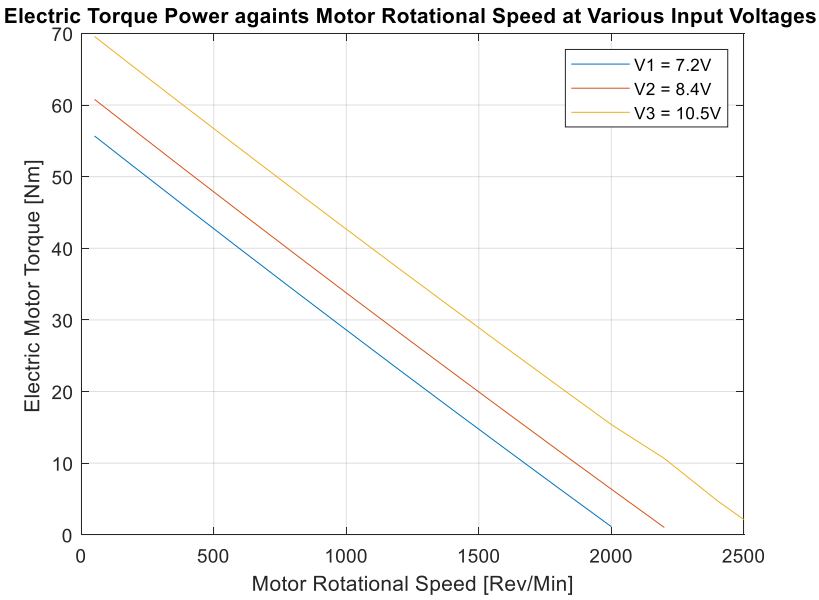


Figure 13: Electric Motor Torque Against Motor Rotational Speed at Various Input Voltages

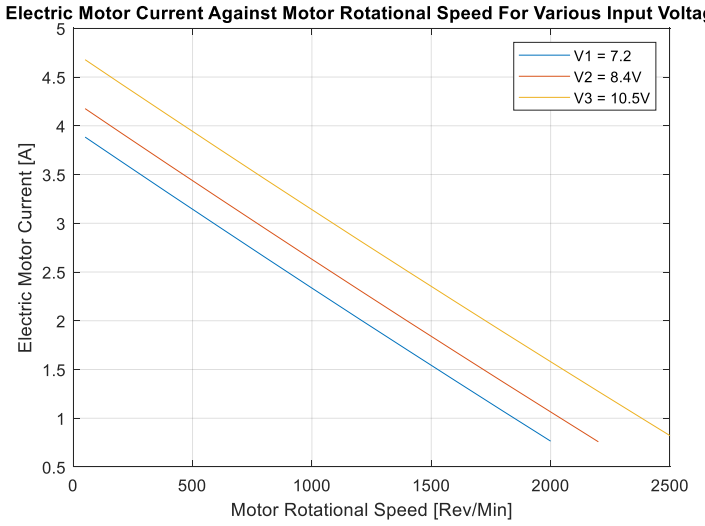


Figure 14: Electric Motor Current Against Motor Rotational Speed at Various Input Voltages

It was not possible to validate the obtained results due to the difficulty of obtaining real experimental data from a manufacturer. However, the results obtained are the same as the results obtained from the theoretical performance of an electric motor obtained by [39][40][41].

2.3. Generator Model

The generator converts mechanical energy from the ICE into electrical energy to recharge the battery. This generally occurs when the propulsion components produce more power than is available for flight during the UAV's mission, resulting in excess power that is converted by the generator into electrical energy to recharge the battery. To replicate the scenario in a UAV simulation, a simplified generator model was implemented using equations from [44], which are defined as follows:

$$P_{elec} = P_{conv} - P_{el}$$

$$P_{conv} = T_{em}\omega_e$$

$$P_{el} = i^2R = \frac{v_b^2}{R}$$

$$v_{gen} = \frac{P_{elec}}{i_c}$$

$$i_c = i - i_0$$

Where: P_{elec} is the electrical power produced by the generator from the ICE, P_{conv} is the power converted to electricity from the ICE, T_{em} is the torque generated by the ICE to charge the battery, ω_e is the motor angular velocity, P_{el} is the electrical power loss due to the motor's internal resistance, R is the motor internal resistance, v_b is the motor back emf, v_{gen} is the voltage produced by the generator to charge the battery, i_c is the difference between the terminal current and the no-load current.

2.4. Internal Combustion Engine (ICE) Model:

The ICE was modelled in Matlab – Simulink using engine data from the Aerosonde UAV [42]. It determines the engine ICE power, ICE Torque, Brake Specific fuel consumption, and fuel flow for a given engine throttle, engine atmospheric pressure, engine rotational speed, and temperature at the UAV's reference altitude. Figure 15 shows a Simulink model of the ICE.

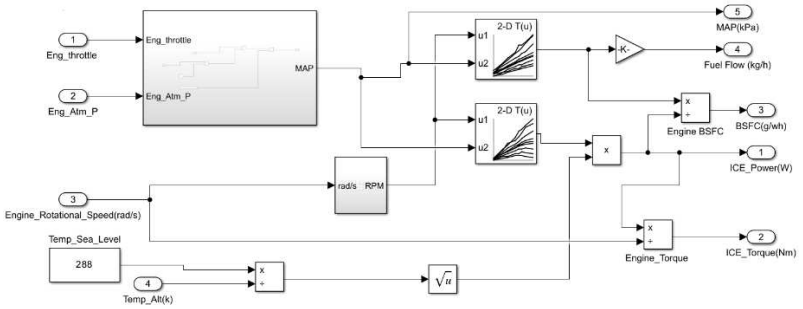


Figure 15: Simulink Model of the ICE

The Manifold Air Pressure (MAP) is determined by the model as:

$$P_{ma} = P_{min} + \left(\frac{P_{atm}}{1000}\right) \times \eta_{th}$$

The ICE power at any given altitude is determined by the model as:

$$P_{ICE,Alt} = P_{ICE}\sqrt{\frac{T_{alt}}{T_{sea_level}}}$$

The engine Brake Specific Fuel Consumption is determined by the model as:

$$BSFC = \frac{FF}{P_{ICE,Alt}}$$

The engine torque is determined from the ICE power and engine rotational speed as:

$$T_{ICE} = \frac{P_{ICE,Alt}}{\omega_{eng}}$$

$Where$: P_{ma} is the engine manifold pressure, P_{min} is the minimum atmospheric pressure, P_{atm} is the engine atmospheric pressure η_{th} is the engine throttle, T_{sea_level} is the temperature at sea level, T_{alt} is the temperature at a given altitude, P_{ICE} is the ICE power, $P_{ICE,Alt}$ is the ICE power at a given altitude, $BSFC$ is the engine Brake Specific Fuel Consumption, FF is the engine fuel flow, T_{ICE} is the ICE torque, ω_{eng} is the engine rotational speed. The model was run at various engine throttle positions to evaluate its effects on the output parameters of the ICE. Figures 16, 17, 18, and 19 show the power, torque, BSFC, and FF curves obtained when the model was run at various engine throttle positions.

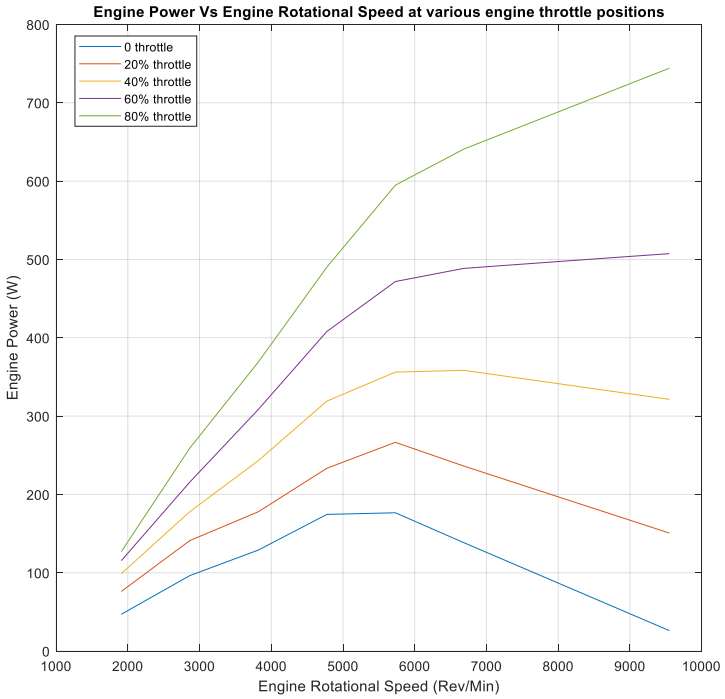
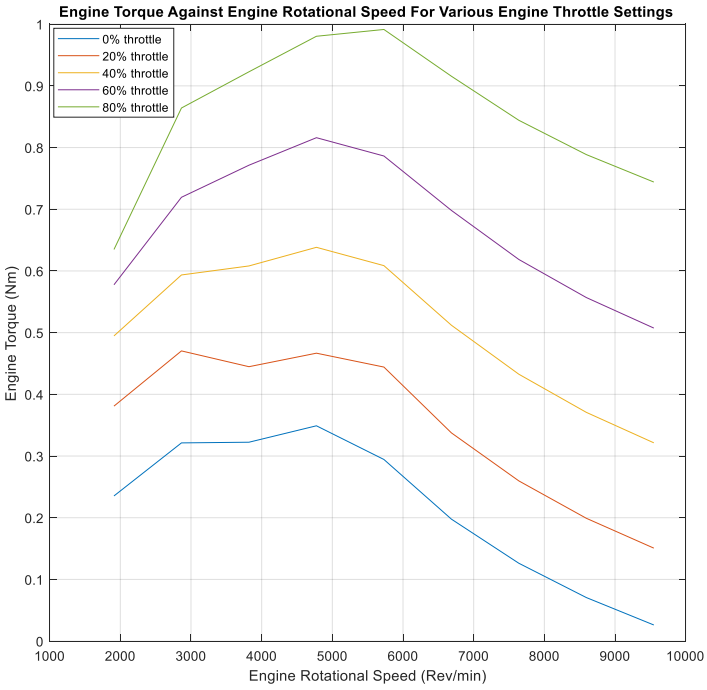
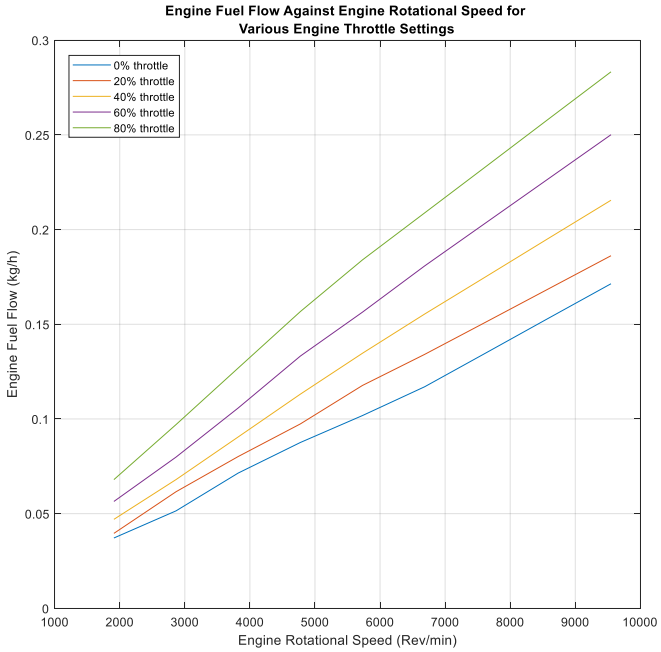


Figure 16: Engine Power Against Engine Rotational Speed at Various Engine Throttle Position



273

274 **Figure 17: Engine Torque Against Engine Rotational Speed at Various Engine Throttle Positions**



275

276 **Figure 18: Engine Brake Specific Fuel Consumption at Various Engine Throttle Positions**

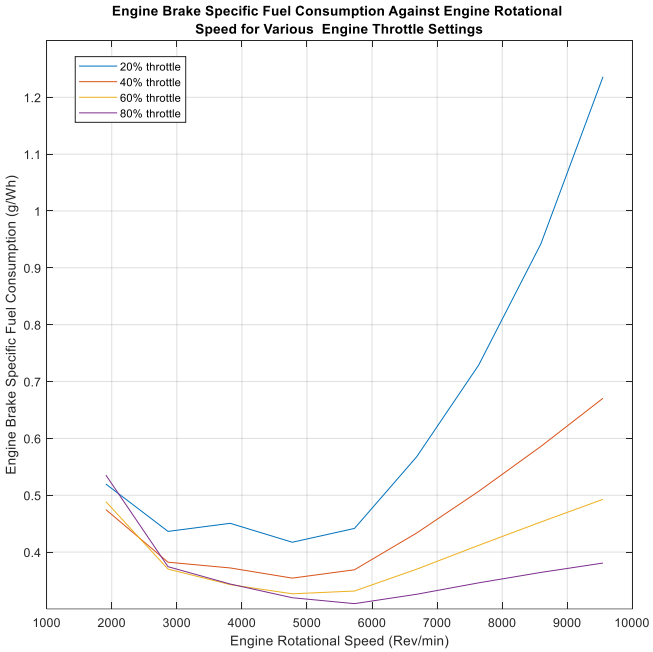


Figure 19: Engine Brake Specific Fuel Consumption Against Engine Rotational Speed at Various Engine Throttle Positions

Figure 20 shows the engine fuel consumption map obtained from the model, which represents the fuel operating range of the ICE for a given torque, engine rotational speed, and Engine BSFC.

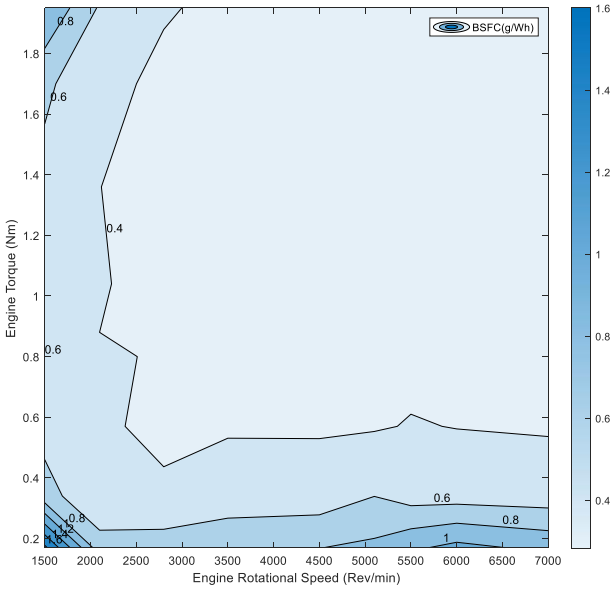


Figure 20: Engine Fuel MAP with BSFC Contours using ICE Data

2.4. Propeller Model

The propeller was modelled using data from an APA 4012 propeller from the University of Illinois Urbana – Champaign (UIUC) propeller database [43]. It determines the propeller thrust, torque,

power, and efficiency for a given propeller diameter, rotational speed, air density, and UAV speed. Figure 21 shows a Simulink model of the propeller.

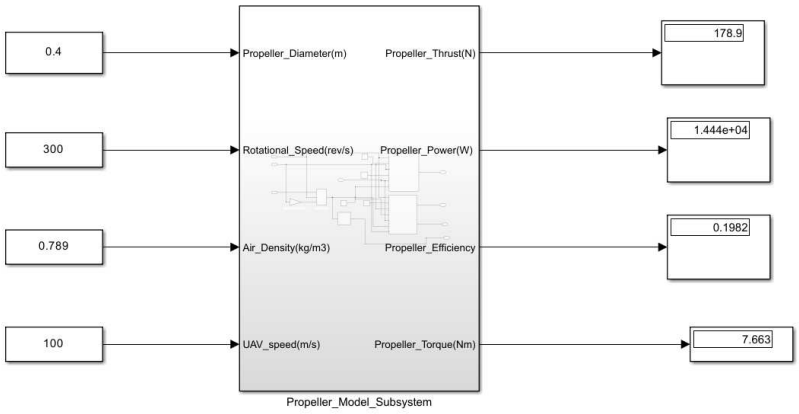


Figure 21: Simulink Model of the Propeller

The propeller modelling equations are given by [44]:

$$J_P = \frac{V}{nD}$$

$$C_T = \frac{T}{\rho n^2 D^4}$$

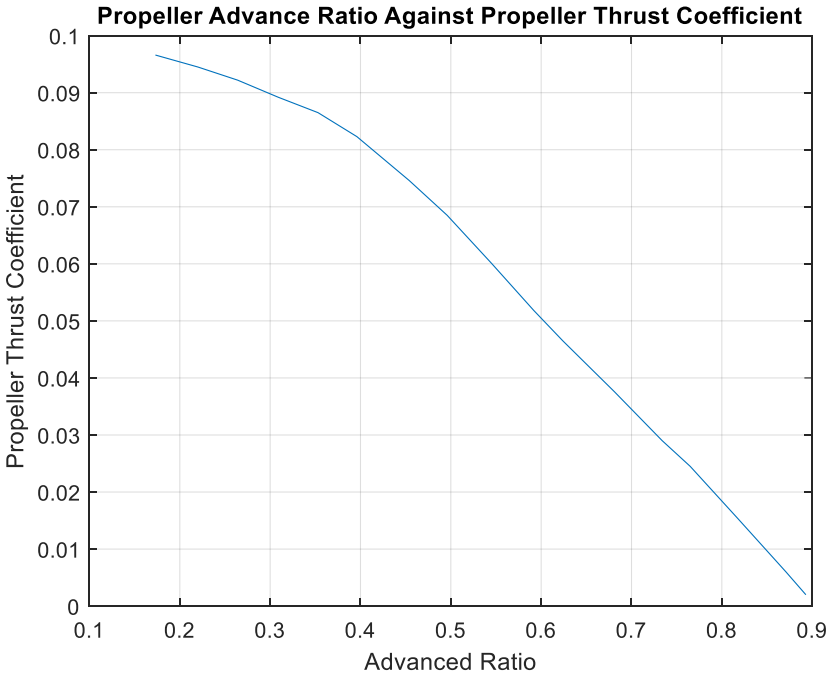
$$C_p = \frac{P}{\rho n^3 D^5}$$

$$Q = \frac{P}{n}$$

$$C_Q = \frac{C_p}{2\pi}$$

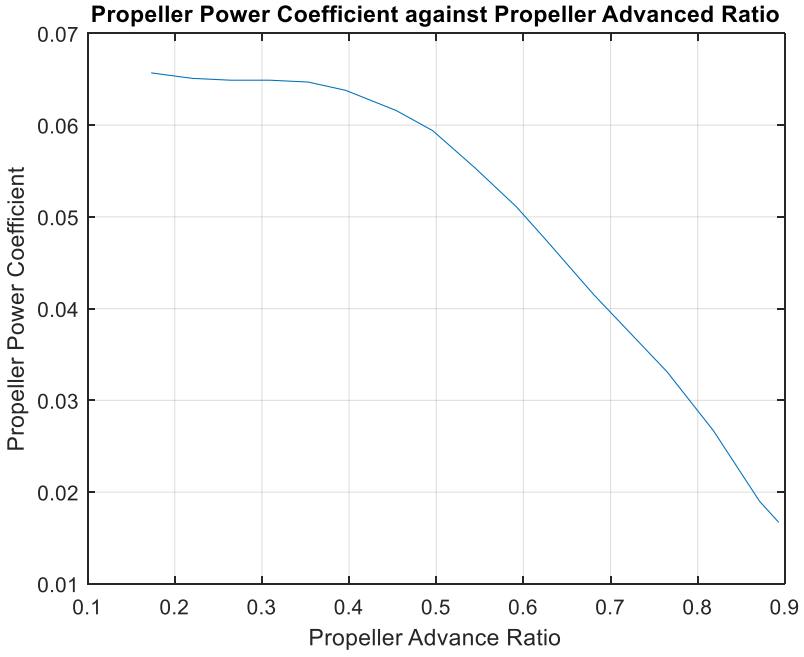
$$\mathrm{C_Q} = \frac{\mathrm{Q}}{\rho \mathrm{n}^3 \mathrm{D}^5 \mathrm{C_Q}}$$

Where: V is the UAV air speed, n is the rotational speed, D is the propeller diameter, C_T is the propeller thrust coefficient, T is the propeller thrust, ρ is the air density, C_p is the propeller power coefficient, P is the propeller power. C_Q is the propeller torque coefficient, Q is the propeller torque. Figure 22, Figure 23 and Figure 24 shows the propeller thrust coefficient, torque coefficient, and efficiency against advanced ratio obtained from the model.



302

303 **Figure 22: Advanced Ratio Against Propeller Thrust Coefficient**



304

305 **Figure 23: Advanced Ratio Against Propeller Power Coefficient**

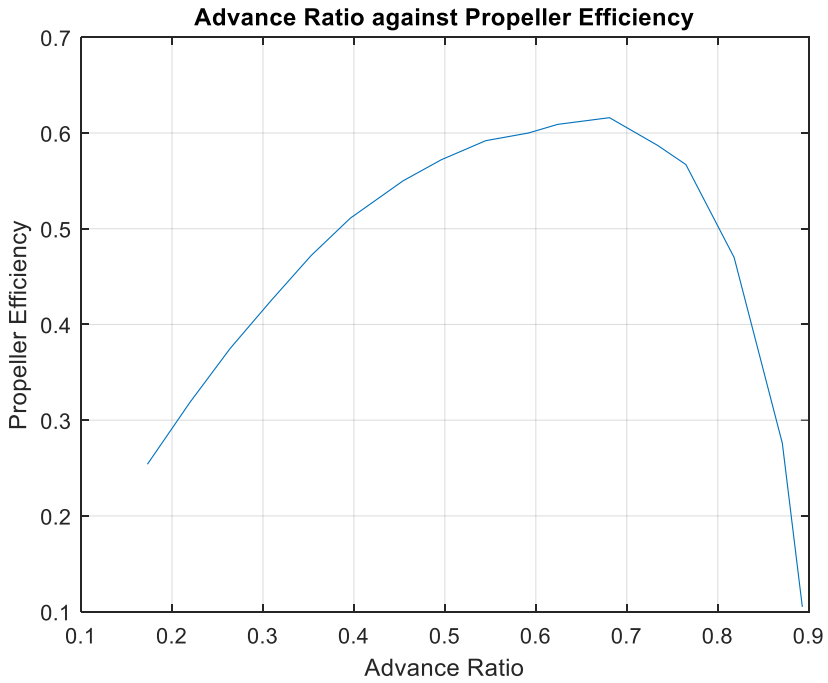


Figure 24: Propeller Advanced Ratio Against Propeller Efficiency

2.5. DC – DC converter Model

Two converters were implemented on Simulink. The buck converter, which steps down the voltage from the propulsion system of the UAV, and boast converter, which steps up the voltage. Their dynamic equations are respectively described as:

Buck converter:

$$\frac{di_L}{dt} = \frac{V_i - V_0}{L}, \quad \frac{dV_0}{dt} = \frac{i_L}{C} - \frac{V_0}{R_L C}$$

$$\frac{di_L}{dt} = -\frac{V_0}{L}, \quad \frac{dV_c}{dt} = \frac{i_L}{C} - \frac{V_c}{R_L C}$$

Boast converter:

$$\frac{di_L}{dt} = -\frac{V_i}{L}, \quad \frac{dV_0}{dt} = -\frac{V_0}{R_L C}$$

$$\frac{di_L}{dt} = \frac{V_i - V_0}{L}, \quad \frac{dV_0}{dt} = \frac{i_L}{C} - \frac{V_0}{R_L C}$$

2.6. Electronic Speed Control (ESC) Model

The electronic speed control model was developed to regulate the rotational speed of the electric motor in the propulsion system of the UAV in simulation. It is described by the following dynamic equations [45]:

$$U_{ESC,max} = U_{mMax}$$

$$I_{ESC,max} = I_{mMax}$$

$$U_{input} = S_{bat}.3.7$$

$$PWF = \frac{I_M U_M}{U_{ESC,max} I_{ESC,max}}$$

$$\eta_{ESC} = \left(U_{input} - R_{bat} - PTF(1 - PWF)\right) / U_{input}$$

$$P_{ESC} = I_M U_M$$

$$I_{ESC} = \frac{(P_{ESC}/\eta_{ESC})}{U_{input}}$$

2.7. Fuel System Model

The Fuel burn model was implemented in Simulink to estimate the fuel burn during the mission of the UAV. The model determines the amount of fuel burn for a given drag force, airspeed, specific fuel consumption, and propeller efficiency. Figure 25 shows the Simulink model of the fuel subsystem.

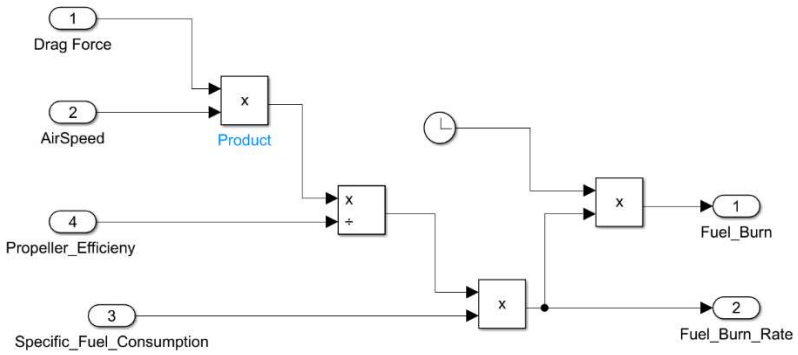


Figure 25: Fuel Burn Simulink Model

The power available for propulsion is determined by the model as:

$$P_{ava} = D \times V$$

Where: D is the drag produced by the UAV and V is the airspeed

The actual power produced by the UAV is always greater than the available power due to the wasted kinetic energy in the air produced by the UAV, which adds to the available power to produce the actual propulsive power of the UAV [46]. To account for the additional power due to the kinetic energy lost in the air, an efficiency factor is introduced in the model such that the actual power generated by the UAV is determined as:

$$P_{eng} = \frac{P_{ava}}{\eta}$$

Where: η is the propulsive efficiency

The fuel burn rate is determined by the model as:

$$\dot{m}_f = P_{gen} \times BSFC$$

The mass of fuel burn is determined by the model as:

$$m_f = \int_0^t \dot{m}_f \, dt$$

2.8. UAV Model

The UAV model was developed in Simulink by considering the 3-dimensional motion of a point mass in steady accelerated flight, as shown in Figure 26.

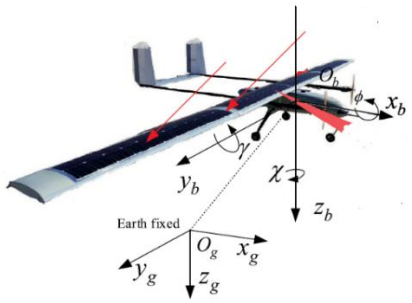


Figure 26: Fixed Wing UAV Diagram [12]

x_b, y_b, z_b are the coordinates of the body frame of the aircraft, x_g, y_g, z_g are the coordinates of the fixed earth frame. The dynamic equations of the aircraft are defined as [47]:

$$\dot{r}_x = V cos(\gamma) cos(\chi)$$

$$\dot{r}_y = V cos(\gamma) sin(\chi)$$

$$\dot{r}_h = V sin(\gamma)$$

$$\dot{V} = \left(\frac{T - \dot{D}}{mg} - sin(\gamma) \right) g$$

$$\dot{\gamma} = \left(\frac{L cos(\varphi)}{mg} - cos(\gamma) \right) \frac{g}{V}$$

$$\dot{\chi} = \frac{L sin(\varphi)}{mV cos(\gamma)}$$

Where: (r_x, r_y, h_z) denotes the axial, lateral, and vertical position of the UAV, respectively, $\dot{r}_x, \dot{r}_y$ are the velocities of the UAV in the axial and lateral directions, $\dot{r}_h$ is the rate of climb of the UAV. V is the velocity of the UAV, γ is the angle of climb, χ is the heading angle, $\dot{V}$ is the acceleration of the UAV, T is the UAV Thrust, D is the UAV drag, m is the mass of the UAV, g is the acceleration due to gravity, L is the lift of the UAV, φ is the bank angle, $\dot{\gamma}$ is the rate of climb angle, $\dot{\chi}$ is the rate of heading angle. The lift and drag can be calculated by the model according to aerodynamic theory as:

$$L = \frac{1}{2}\rho V^2 S C_L$$

$$D = \frac{1}{2}\rho V^2 S C_D$$

Where: S is the wing reference area, ρ is the atmospheric density, C_L is the lift coefficient, C_D is the drag coefficient. C_d can also be expressed in terms of the parasite drag coefficient C_{d0} and aerodynamic coefficient k_e as:

$$C_D = C_{D0} + k_e C_L^2$$

And k_e is expressed in terms of aspect ratio R_a and Oswald factor ϵ as:

$$k_e = \frac{1}{\epsilon \pi R_a}$$

The equations were used to develop a Simulink model of the UAV, which was used to estimate the fuel consumption of the developed powertrain model at any given time step. The model determines the lift force, drag force, rate of climb, axial velocity, lateral velocity, angle of climb, heading angle, bank angle, rate of angle of climb, and thrust force for a given airspeed and atmospheric density. The parameters for the UAV model were obtained from the Aerosonde UAV [48][49], which has the following characteristics as shown in Table 1.

Parameters	Value	Unit
Length, a	1.74	m
Wingspan, b	2.9	m
Wing area, S	0.55	m^2
Mass, m	13.5	kg
Aspect Ratio, AR	15.3	-
Lift Coefficient, $C_L^{\propto}$	5.61	-
Zero Lift Coefficient, C_{L0}	0.23	-

Parasite Drag Coefficient, C_{D0}	0.0434	-
Propeller Efficiency, η_{prop}	0.75	-
Motor Efficiency, η_{motor}	0.8	-

Table 1: Main Parameters of Hybrid Electric Aerosonde [14]

2.9. Clutch Model

A simplified clutch model was developed to couple the energy from the propulsion system to the propeller of the aircraft, which is defined as follows:

$$T_{out} = \begin{cases} T_{ICE} + T_{EM} \; if \; the \; clutch \; is \; engaged \\ 0 \; if \; the \; clutch \; is \; disengaged \end{cases}$$

$$\omega_{out} = \begin{cases} max(\omega_{ICE} + \omega_{EM}) \; if \; the \; clutch \; is \; engaged \\ \omega_{EM} \; if \; clutch \; is \; disengaged \; and \; EM \; driven \\ \omega_{ICE} \; if \; clutch \; is \; disengaged \; and \; ICE \; driven \end{cases}$$

It should be noted that the clutch is engaged when the rotor of the electric motor and the plate of the ICE make contact to transfer power, and the clutch is disengaged when the rotor and plate do not make contact.

3. Architectures Configuration

Four main architecture models of the UAV were implemented on Simulink which are: Electric Configuration, Conventional Configuration, Serial Hybrid Electric Configuration, and Parallel Hybrid Electric Configuration.

3.1. Electric Architecture

Figure 27 shows the Simulink model of the electric architecture where only the electric motor powers the propeller of the aircraft in flight.

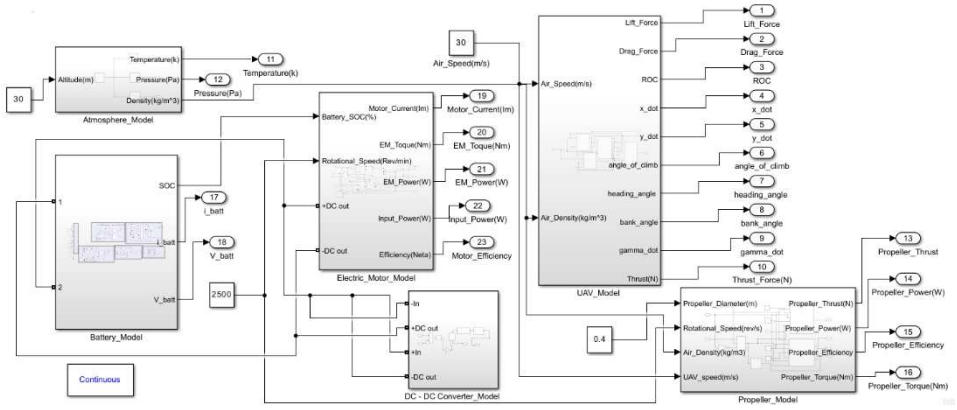


Figure 27: Electric Powertrain Architecture of the UAV

3.2. Conventional Architecture

Figure 28 shows the Simulink model of a conventional architecture where only the ICE drives the propeller of the aircraft in flight.

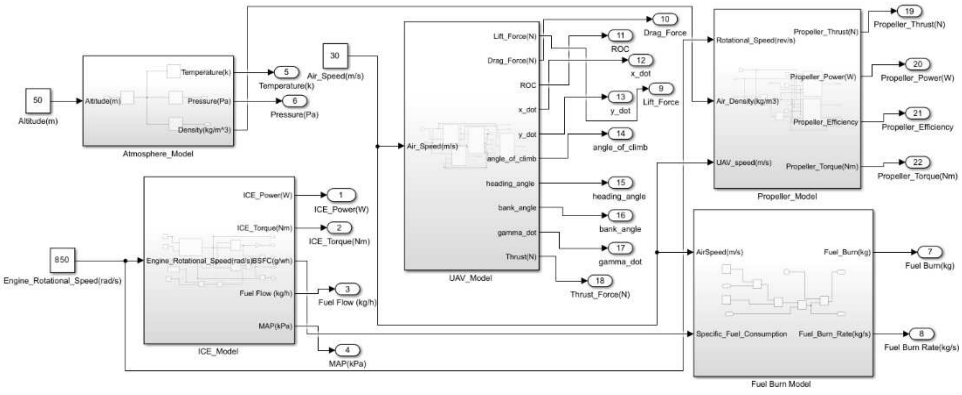


Figure 28: Conventional Powertrain Architecture of the UAV

3.3. Serial Hybrid Electric Architecture

Figure 29 shows the Simulink model of the serial hybrid electric architecture of the UAV, where the electric motor drives the propeller of the aircraft, which is assisted by the generator through the ICE and the generator, which recharges the battery in flight.

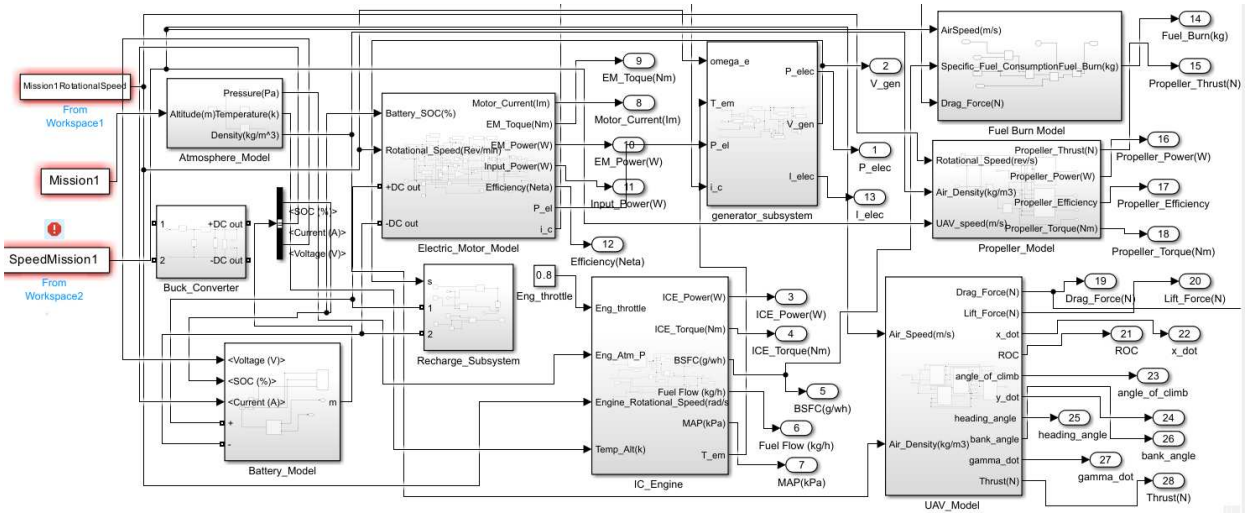


Figure 29: Serial Hybrid Electric Architecture of the UAV

3.4. Parallel Hybrid Electric Architecture

Figure 30 shows the Simulink model of the parallel hybrid electric architecture of the UAV, where both the electric motor and ICE drive the propeller in flight.

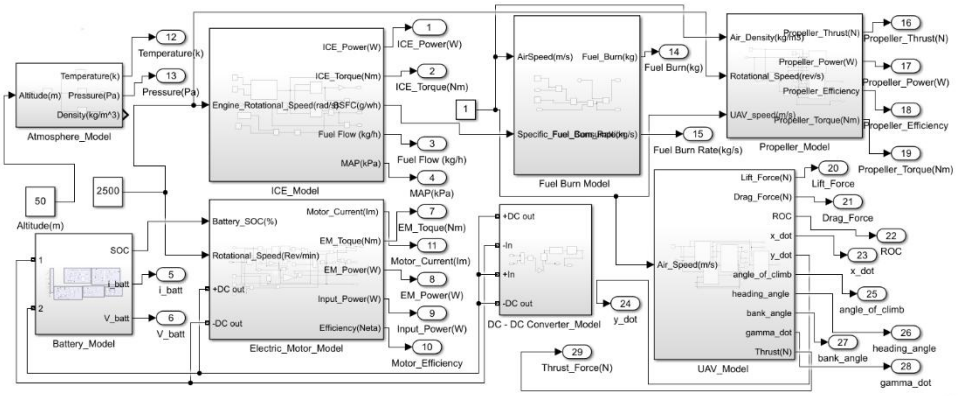


Figure 30: Parallel Hybrid Electric Architecture of the UAV

4. Rule-Based Controlled Strategy

Two rule-based control strategies of the hybrid UAV were designed for the serial architecture and for the parallel architecture of the UAV. These are described below:

4.1. Rule-Based Control Strategy for the Parallel Architecture

The formulation of the rule-based controlled strategy for the parallel hybrid architecture of the UAV was based on five different flight stages along the mission of the aircraft, which are defined as follows:

Stage 1: Hybrid Mode (Take-off and Climb), which happens when the aircraft uses energy from both the ICE and EM.

$$P(t) = P_{ICE}(t) + P_{EM}(t)$$

$$T(t) = T_{ICE}(t) + T_{EM}(t)$$

Stage 2: ICE-only Mode (Cruise): When the aircraft transitions to stage 2, it uses energy only from the ICE.

$$P(t) = P_{ICE}(t), P_{EM}(t) = 0$$

$$T(t) = T_{ICE}(t), T_{EM}(t) = 0$$

Stage 3: Hybrid Mode (Cruise): During stage 3, the aircraft uses energy from both the ICE and EM

$$P(t) = P_{ICE}(t) + P_{EM}(t)$$

$$T(t) = T_{ICE}(t) + T_{EM}(t)$$

Stage 4: ICE only Mode (Cruise): In stage 4, the aircraft uses energy only from the ICE

$$P(t) = P_{ICE}(t), \qquad P_{EM}(t) = 0$$

$$T(t) = T_{ICE}(t), \qquad T_{EM}(t) = 0$$

Stage 5: ICE only Mode (Descend and Landing): In this stage , the aircraft uses energy only from the ICE.

$$P(t) = P_{ICE}(t), \qquad P_{EM}(t) = 0$$

$$T(t) = T_{ICE}(t), \qquad T_{EM}(t) = 0$$

4.2. Rule-Based Controlled Strategy for the Serial Architecture

Stage 1: Hybrid Mode (Take-off and Climb)

$$P(t) = P_{EM}(t) + P_{gen}(t)$$

$$T(t) = T_{EM}(t) + T_{gen}(t)$$

Stage 2: Generator Mode (cruise)

$$P(t) = P_{Gen}(t), P_{EM}(t) = 0$$

$$T(t) = T_{Gen}(t), T_{EM}(t) = 0$$

Stage 3: Hybrid Mode (Cruise Mode)

$$\mathrm{P(t)} = \mathrm{P_{gen}(t)} + \mathrm{P_{EM}(t)}$$

$$\mathrm{T(t)} = \mathrm{T_{gen}(t)} + \mathrm{T_{EM}(t)}$$

Stage 4: EM Mode (Endurance)

$$P(t) = P_{EM}(t), \qquad P_{Gen}(t) = 0$$

$$T(t) = T_{EM}(t), \quad T_{Gen}(t) = 0$$

Stage 5: Hybrid Mode (Cruise)

$$P(t) = P_{Gen}(t) + P_{EM}(t)$$

$$T(t) = T_{Gen}(t) + P_{EM}(t)$$

Stage 6: Generator Mode (Descend and Landing)

$$P(t) = P_{Gen}(t), \qquad P_{EM}(t) = 0$$

$$T(t) = T_{Gen}(t), \qquad T_{EM}(t) = 0$$

5. Results and Discussion

5.1. Inputs

The model's inputs are the mission altitude, rotational speed, and mission speed.

5.2. Mission Altitude

The mission altitude comprises of a 3-hour Intelligence Surveillance and Reconnaissance (ISR) mission used for military application where the aircraft takes off and climbs to an altitude of 500m, cruises at constant altitude of 500m, transitions to a higher altitude at 700m, then to a lower altitude of 350m and finally cruises at constant altitude 650m ontill it reaches the descend and landing phases as shown in figure 31.

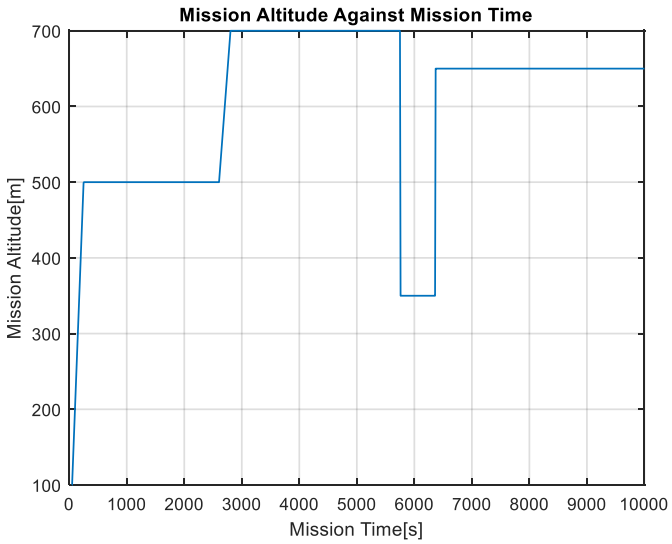


Figure 31: Mission Altitude Against Time of the UAV

5.3. Mission Rotational Speed

The rotation speed of the ICE increases to a maximum speed of 4500 rev/min during takeoff and climb, remains constant at 4500 rev/min during the cruising phase, then transitions to a lower rotation speed of 3500 rev/min in the next cruising phase, then 800 rev/min in the endurance phase and finally peaks up again to a higher speed of 4500 rev/min in the last mission phase as shown in figure 32.

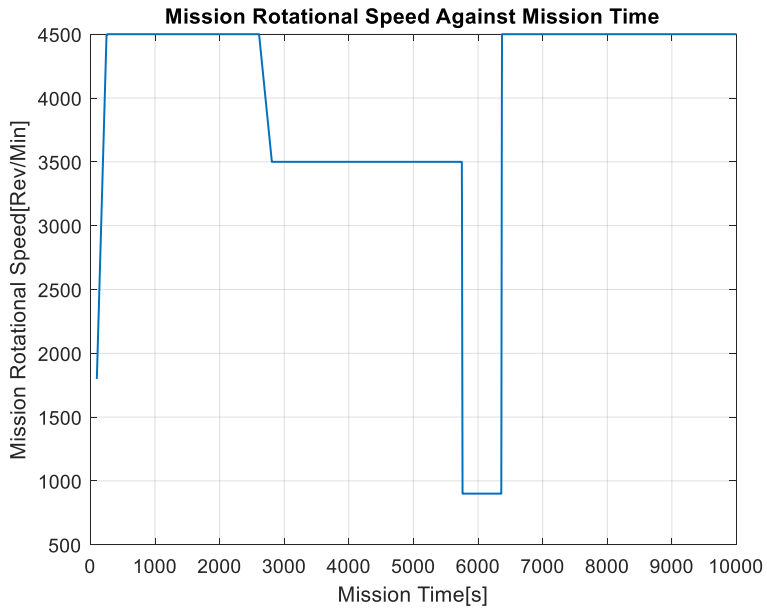


Figure 32: Mission Rotational Speed Against Mission Time of the UAV

5.4. Mission Speed

The speed of the aircraft increases to a maximum speed of 20m/s during the take-off and landing phase and remains constant at 20m/s during the remaining mission phases of the aircraft, as shown in Figure 33.

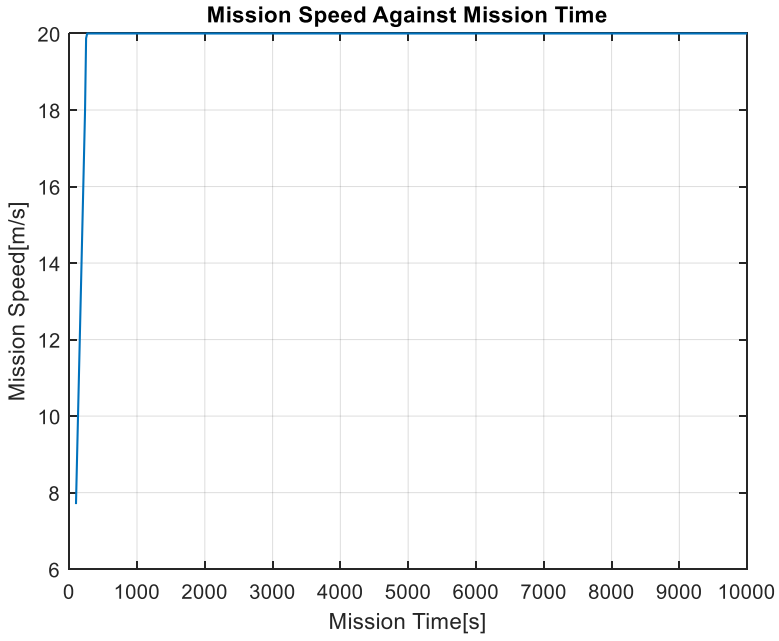


Figure 33: Mission Speed Against Mission Time of the UAV

5.5. ICE power

Figure 34 shows the power variation from the ICE along the mission of the aircraft when only the ICE is used, which increases up to a maximum value of 570W when the aircraft is climbing to an altitude of 500m and remains constant during the cruising phase. The power decreases to 395W when the aircraft cruises at a lower rotational speed of 3500rev/min and at a higher altitude of 700m, and peaks up again to 550W when the aircraft cruises at a higher rotational speed of 4500rev/min.

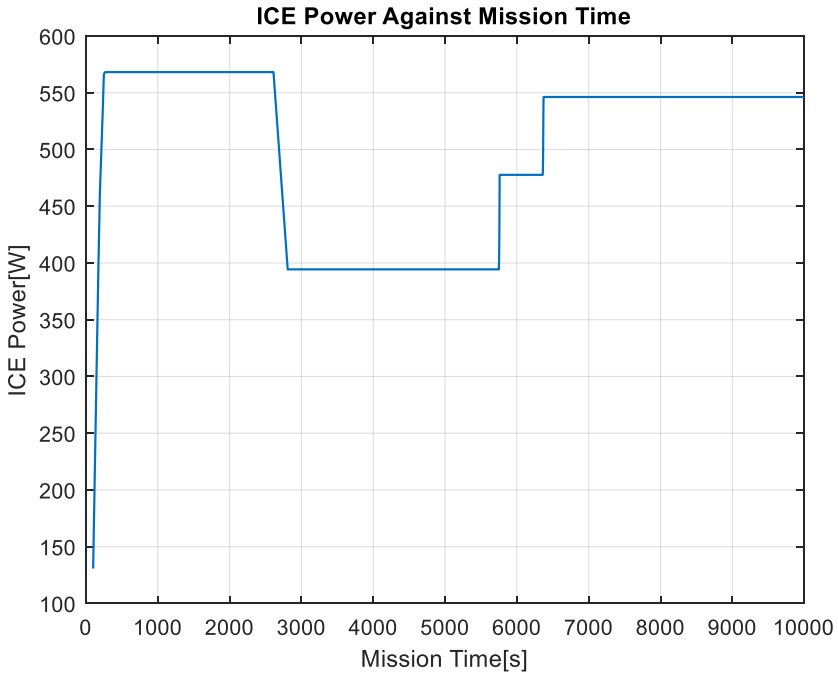


Figure 34: ICE Power Against Mission Time of the UAV

5.6. ICE Torque

Figure 35 shows the torque variation of the ICE along the different mission phases of the aircraft when only the ICE is used.

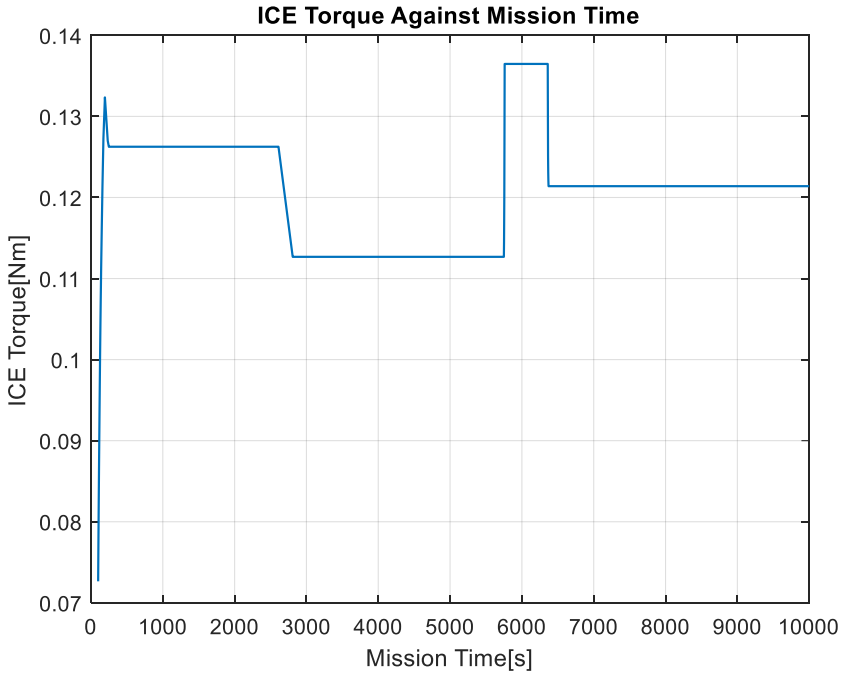


Figure 35: ICE Torque Against Mission Time of the UAV

5.7. ICE BSFC

Figure 36 shows the BSFC variation of the ICE along the whole mission of the aircraft when only the ICE is used.

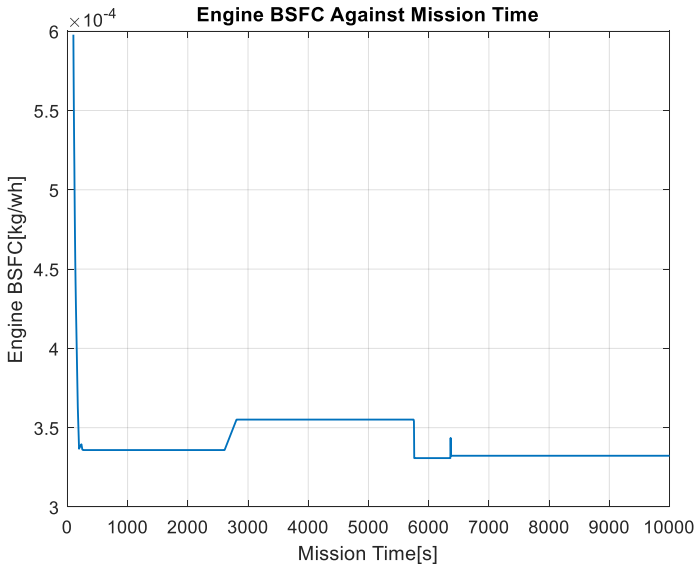
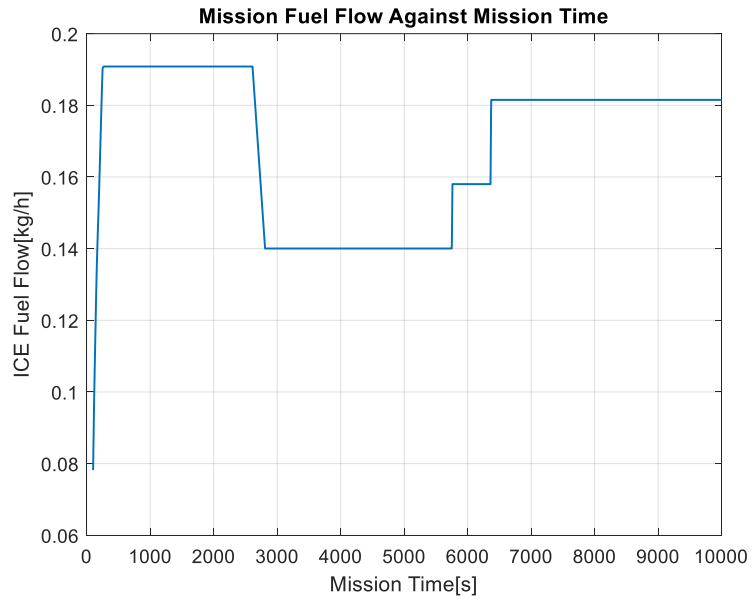


Figure 36: Engine BSFC Against Mission Time of the UAV

5.8. ICE Fuel Flow

Figure 37 shows the fuel flow variation of the ICE along the whole mission of the aircraft when only the ICE is used.



508

509 **Figure 37: Engine fuel flow Against Mission Time of the UAV**

510 ## 5.9. Mission Power (Energy Management Analysis Using Rule-Based Controlled
511 Strategy)

512 Figure 38 shows the power used along the mission by the hybrid propulsion system of the UAV.
513 During take-off and climb, the power peaks up to a maximum value of 2500W when the UAV is climb-
514 ing, which is achieved by the propulsion system operating in hybrid mode. The power then decreases
515 to 515W when the UAV is operating in ICE mode between 260s and 2650s during the first cruising
516 stage, and peaks up again to about 2100W when the UAV is operating in hybrid mode between 2660s
517 and 5750s in the second cruising stage. The power then decreases again to about 550W in the re-
518 maining mission phases of the aircraft. It is important to note that the power decreases during the
519 cruising stage since more power is required in the climbing mission phase than in the cruising stage.
520 An estimate of the power required to satisfy the mission of the UAV was determined using power
521 profile curves used by previous researchers from literature [50], as shown in figure 38. Also, it is ob-
522 served that mission power satisfies the power required of the aircraft throughout its mission. Some
523 spikes are also observed as a result of the controller trying to change operating mode during the
524 mission of the aircraft [48], which is also a result of the aircraft changing speed [44].

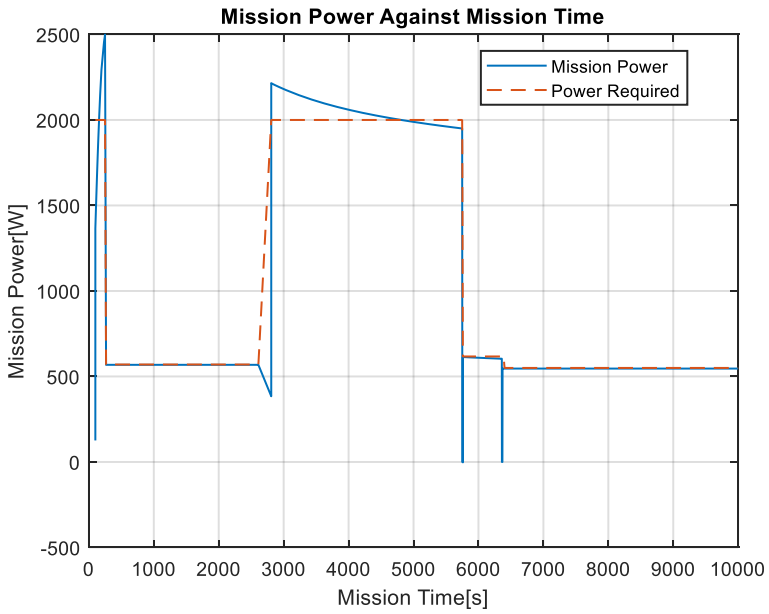


Figure 38: Mission Power Against Mission Time

5.10. Mission Torque Required

Figure 39 shows the torque used along the mission by the hybrid propulsion system of the UAV. It is observed that the torque is low during certain mission segments where the UAV uses the combustion engine, and peaks when the UAV uses both power sources.

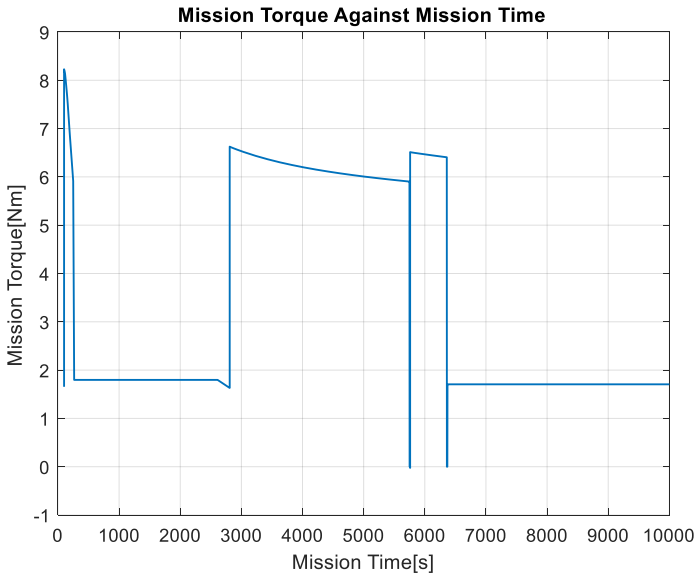


Figure 39: Mission Against Mission Time

5.11. EM Power

Figure 40 shows the electric motor power variation along the whole mission of the aircraft. It can be observed that the electric motor remains silent over certain mission segments of the aircraft. The

electric motor power is zero over these mission segments of the aircraft since only the ICE powers the aircraft.

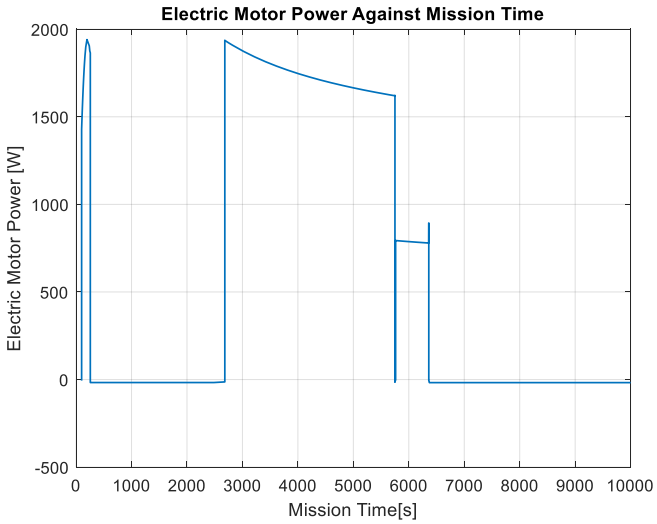


Figure 40: Electric Motor Power Variation Against Mission Time of the UAV

5.12. EM Torque

Also, the electric motor torque is silent during these mission segments of the aircraft since only the ICE powers the aircraft, and the electric motor torque is zero during these mission segments, as shown in Figure 41.

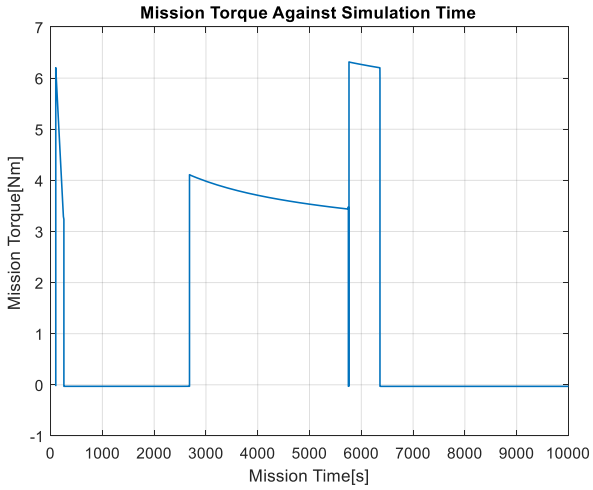


Figure 41: Electric Motor Torque Variation Against Mission Time of the UAV

5.13. Motor Current

Figure 42 shows the motor current draw from the EM throughout the mission of the aircraft, which peaks up to a maximum value of 0.16A during the climb segment and changes throughout the different mission phases of the aircraft. It also observed that the motor current is zero during some mission segments of the aircraft, where only the ICE is used.

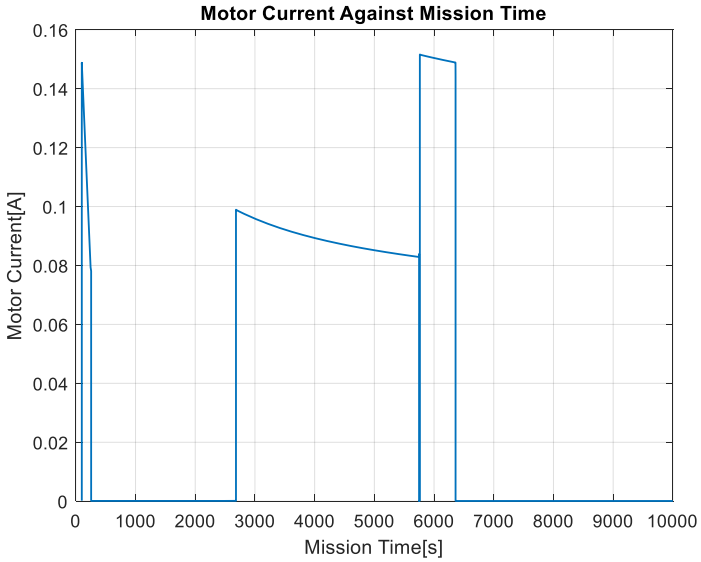


Figure 42: Motor Current Variation Against Mission Time of the UAV

5.14. Battery SOC

Figure 43 shows the battery SOC along the whole mission of the UAV. The battery SOC is constant during some mission segments where only the ICE is used, and decreases during the mission segments where the electric motor is used.

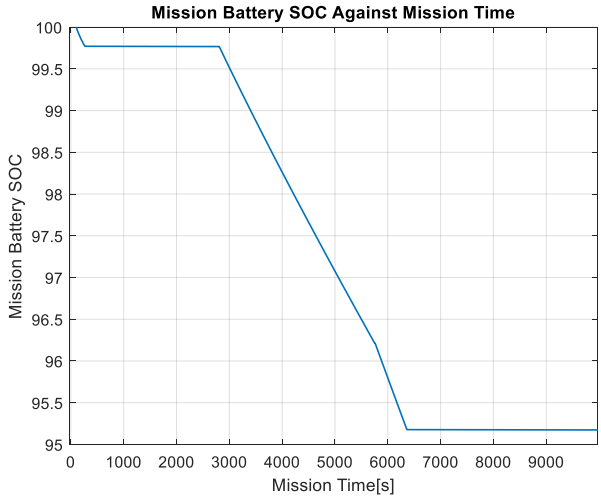


Figure 43: Battery SOC Against Mission Time

5.15. Mission Fuel Burn

Figure 44 shows the fuel burn along the mission for the ICE-powered UAV and the hybrid-powered UAV. It is observed that the ICE-powered UAV uses more fuel than the hybrid-powered UAV over the same mission profile. The hybrid UAV achieves a fuel burn of 4.2kg, while the ICE-powered UAV achieves 5.4kg for the same mission.

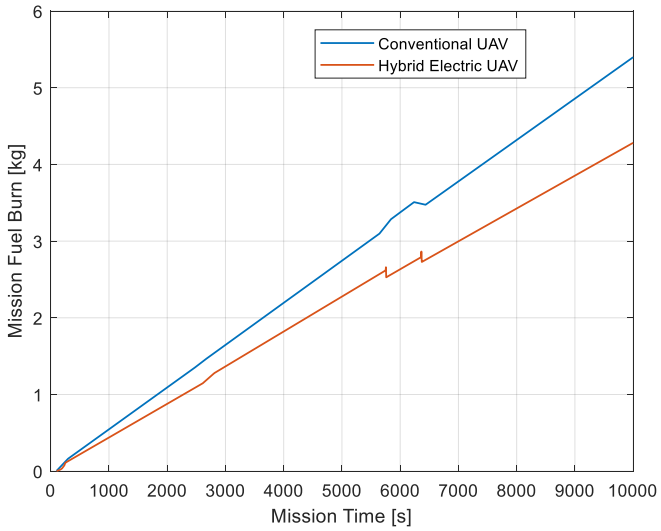


Figure 44: Mission Fuel Burn Against Mission Time

Figure 45 shows the variation of the thrust and drag force along the whole mission of the aircraft. The thrust force increases during the takeoff and climbing phase of the aircraft since more propulsive power is needed, which is achieved with the ICE and EM working together, and it remains steady throughout the mission of the aircraft. It can be observed that the thrust of the UAV matches the drag at all the mission phases of the aircraft since steady unaccelerated flight was considered when developing the model.

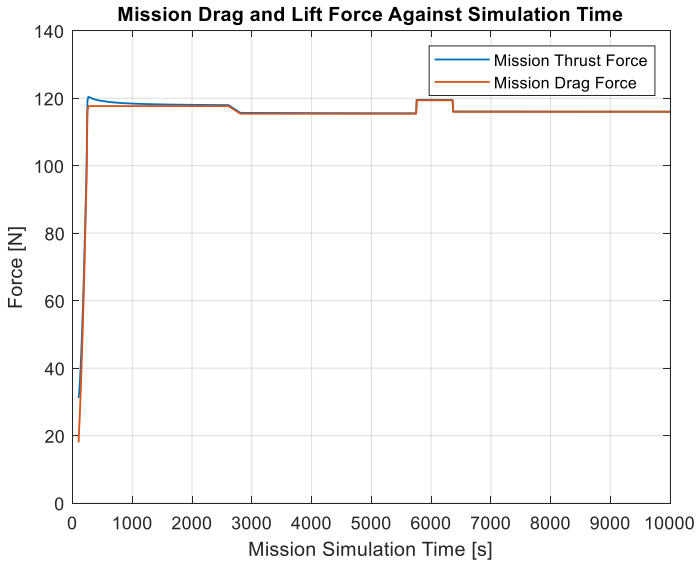


Figure 45: Mission Force Against Mission Time

5.16. Fuel Burn Comparison between Parallel Hybrid Architecture and Conventional Architecture

Various ISR mission profiles consisting of various mission segments were varied to evaluate the fuel burn achieved by the UAV. Table 2 gives the fuel burn and the percentage of fuel consumption reduction achieved compared to the conventional powertrain system for each ISR mission type. The fuel burn increased as the mission time increased, with the percentage of fuel burn improvement changing slightly, i.e 22.9%, 19.1% and 22.2% for Mission 1, Mission 2, and Mission 3, respectively. Table 3 shows the parameter specifications of the propulsive components of the UAV used when developing the model.

ISR Mission Time(h)	Mission Segments	Mass of Fuel Burn For Conventional Architecture (kg)	Mass of fuel burn for parallel hybrid Architecture (kg)	Percentage of fuel consumption reduction (%) compared to conventional architecture
1h	Take-off and climb, cruise, cruise, descend, and landing	2.05	1.58	22.9
2h	Take-off and climb, cruise, cruise, cruise, descend, and landing	4.14	3.35	19.1

3h	Take-off and climb, cruise, cruise, cruise, cruise, descend and landing	5.4	4.2	22.2

586 **Table 2: Fuel Burn Comparison Table Between Parallel Hybrid Architecture and Conventional Architecture**

Propulsion System Component	**Parameter Specification**
Battery	Nominal Voltage: 20V Rated Capacity: 2.5Ah Initial SOC: 100 Battery Response Time: 30 Maximum Capacity: 2.5Ah Cut-off Voltage: 15V Fully Charged Voltage: 23.3 Nominal Discharge Current: 1.087A Internal Resistance: 0.08Ω
ICE	Sea level temperature: 288K Minimum Engine Atmospheric Pressure: 60kpa Engine Throttle: 0.377
Electric Motor	Motor Speed Constant(k_v): 400 Motor Internal Resistance: 120 Ω

	No-load Current: 0.0008A
Propeller	Propeller Diameter: 0.15m Propeller Type: APA 4012 propeller

Table 3: Parameter specifications for the Propulsion component for the model development

6. Conclusion

In this paper, a novel rule-based control strategy was implemented to evaluate the energy efficiency and fuel consumption reduction on a fixed-wing UAV with HEPS. Various drive components for propulsion of the UAV were individually developed which were integrated for various powertrain architectures. The results obtained were compared with the results obtained for a conventional powertrain system of the UAV. Various Missions profiles were considered. Through simulation, it was shown that a UAV with a parallel hybrid electric propulsion system saved about 22% of fuel compared to a conventional powertrain system. Further research will investigate other supervisory control strategies to achieve more energy saving, payload capacity, fuel consumption improvement, and battery SOC. An experimental aircraft test facility will also have to be developed to test the developed technology.

References

[1]Ye, X.I.E., Savvarisal, A., Tsourdos, A., Zhang, D. and Jason, G.U., 2021. Review of hybrid electric-powered aircraft, its conceptual design and energy management methodologies. Chinese Journal of Aeronautics, 34(4), pp.432-450.

[2]Li, Y., Liu, L., Ma, X. and Tu, H., 2012, July. Design of a hybrid electric propulsion system for long endurance small UAV. In 10th International Energy Conversion Engineering Conference (p. 4241).

[3] Gong, A., MacNeill, R., Verstraete, D. and Palmer, J.L., 2018, July. Analysis of a fuel-cell/battery/supercapacitor hybrid propulsion system for a UAV using a hardware-in-the-loop flight simulator. In 2018 AIAA/IEEE electric aircraft technologies symposium (EATS) (pp. 1-17). IEEE.

[4] Wang S, Economou J, Tsourdos A. Indirect engine sizing via distributed hybrid-electric unmanned aerial vehicle state-of-charge-based parametrisation criteria. Proceedings of the Institution of Mechanical Engineers, Part G: Journal of Aerospace Engineering. 2019;233(14):5360-5368. doi:10.1177/0954410019843722.

[5] Kurt, Emre, et al. "Parallel hybrid propulsion system with integration of designed electric machine for medium altitude long endurance UAV." Heliyon 11.4 (2025).

[6] Available online: https://news.nationalgeographic.com/energy/2015/04/150409-epa-aviation-emissionsrules-for-airplanes/ (accessed on 16 February 2026).

[7] Harmon, Frederick G. Neural network control of a parallel hybrid-electric propulsion system for a small unmanned aerial vehicle. University of California, Davis, 2005.

[8] Koster, J., Velazco, A., Munz, C. D., Kraemer, E., Wang, K. C., & Verstraete, D. (2012, January). HYPERION UAV: an international collaboration. In 50th AIAA Aerospace Sciences Meeting including the New Horizons Forum and Aerospace Exposition (p. 1223).

[9] Verstraete, Dries, Luigi Cazzato, and Giulio Romeo. "Preliminary design of a fuel-cell-based hybrid-electrical UAV." *Proc. 28th Congress of the International Council of the Aeronautical Sciences*. 2012.

[10] Gong, A., MacNeill, R., Verstraete, D. and Palmer, J.L., 2018, July. Analysis of a fuel-cell/battery/supercapacitor hybrid propulsion system for a UAV using a hardware-in-the-loop flight simulator. In 2018 AIAA/IEEE electric aircraft technologies symposium (EATS) (pp. 1-17). IEEE.

[11] Savvaris, A., Xie, Y., Malandrakis, K., Lopez, M. and Tsourdos, A., 2016, June. Development of a fuel cell hybrid-powered unmanned aerial vehicle. In 2016 24th mediterranean conference on control and au tomation (MED) (pp. 1242-1247). IEEE.

[12] https://www.aeroexpo.online/prod/quaternium-technologies-sl/product-185795-41091.html

[13] https://free3d.com/3d-model/rq-14-dragon-eye-8027.html

[14] https://www.flightglobal.com/lockheed-to-perform-first-uk-flight-of-desert-hawk-uav/82873.article

[15]Tao, L. E. I., Y. A. N. G. Zhou, L. I. N. Zicun, and Xiaobin Zhang. "State of art on energy management strategy for hybrid-powered unmanned aerial vehicle." Chinese Journal of Aeronautics 32, no. 6 (2019): 1488-1503.

[16] Wang, B., Zhao, D., Li, W., Wang, Z., Huang, Y., You, Y. and Becker, S., 2020. Current technologies and challenges of applying fuel cell hybrid propulsion systems in unmanned aerial vehicles. Progress in Aerospace Sciences, 116, p.100620

[17] Aksland, C. T. (2019). Modular modeling and control of a hybrid unmanned aerial vehicle's powertrain (Doctoral dissertation, University of Illinois at Urbana-Champaign).

[18] Xiao, Chunwu, et al. "Comprehensive investigation on Lithium batteries for electric and hybrid-electric unmanned aerial vehicle applications." Thermal Science and Engineering Progress 38 (2023):

[19] Frosina, Emma, Adolfo Senatore, Luka Palumbo, Giuseppe Di Lorenzo, and Ciro Pascarella. "Development of a lumped parameter model for an aeronautic hybrid electric propulsion system." Aerospace 5, no. 4 (2018): 105.

[20] Donateo, Teresa, Antonio Ficarella, and Luigi Spedicato. "A method to analyze and optimize hybrid electric architectures applied to unmanned aerial vehicles." Aircraft Engineering and Aerospace Technology 90.5 (2018): 828-842.

[21]B. M. Baumann, G. Washington, B. C. Glenn, and G. Rizzoni, “Mechatronic design and control of hybrid electric vehicles,” IEEE/ASME Transactions on Mechatronics, vol. 5, no. 1, pp. 58–72, 2000.

[22] N. J. Schouten, M. A. Salman, and N. A. Kheir, "Fuzzy logic control for parallel hybrid vehicles," IEEE Transactions on Control Systems Technology, vol. 10, no. 3, pp. 460–468, 2002.

[23] L. V. Perez, G. R. Bossio, D. Moitre, and G. O. Garcıa, "Optimization of power management in an hybrid electric vehicle using dynamic programming," Mathematics and Computers in Simulation, vol. 73, no. 1–4, pp. 244–254, 2006.

[24] He, Cheng, Yuhong Jia, and Dongli Ma. "Optimization and analysis of hybrid electric system for distributed propulsion tilt-wing UAV." IEEE Access 8 (2020): 224654-224667.

[25] Donateo, T. and Spedicato, L., 2017. Fuel economy of hybrid electric flight. *Applied energy*, *206*, pp.723-738.

[26] Hung, J.Y. and Gonzalez, L.F., 2012. On parallel hybrid-electric propulsion system for unmanned aerial vehicles. *Progress in Aerospace Sciences*, *51*, pp.1-17.

[27] Wang S, Economou J, Tsourdos A. Indirect engine sizing via distributed hybrid-electric unmanned aerial vehicle state-of-charge-based parametrisation criteria. Proceedings of the Institution of Mechanical Engineers, Part G: Journal of Aerospace Engineering. 2019;233(14):5360-5368. doi:10.1177/0954410019843722.

[28] Xie, Y., Savvaris, A., Tsourdos, A., Laycock, J. and Farmer, A., 2018, March. Modelling and control of a hybrid electric propulsion system for unmanned aerial vehicles. In 2018 IEEE aerospace conference (pp. 1-13). IEEE.

[29] Suti, Aleksander, Gianpietro Di Rito, and Roberto Galatolo. "Climbing performance enhancement of small fixed-wing UAVs via hybrid electric propulsion." 2021 IEEE Workshop on Electrical Machines Design, Control and Diagnosis (WEMDCD). IEEE, 2021.

[30] Hyun, Daeil, Jaeyoung Han, and Seokmoo Hong. "Development of hybrid-powered, sustainable multi-purpose drone system: An analysis model." International Journal of Hydrogen Energy 61 (2024): 762-773.

[31] Wilson, Jamal. Modelling, experimental validation and evaluation of a parallel hybrid-electric propulsion system for small-scale UAVs. Diss. 2024.

[32] Greiser, Collin. "Implementation of a Rule-Based Open-Loop Control Strategy for a Hybrid-Electric Propulsions System on a Small RPA." (2011).

[33] Boggero, L., Corpino, S., De Martin, A., Evangelista, G., Fioriti, M., & Sorli, M. (2019). A virtual test bench of a parallel hybrid propulsion system for UAVs. Aerospace, 6(7), 77.

[34] Matlock, J. M. T. (2019). Evaluation of hybrid-electric propulsion systems for unmanned aerial vehicles (Doctoral dissertation).

[35] Obertino, Daniele. Design and Simulation Study of a Hybrid Electric Propulsion System for a VTOL Tilt-Rotor UAV=. Diss. Politecnico di Torino, 2021.

[36] Tremblay, O., & Dessaint, L. A. (2009). Experimental validation of a battery dynamic model for EV applications. World electric vehicle journal, 3(2), 289-298.

[37] Tremblay, Olivier, Louis-A. Dessaint, and Abdel-Illah Dekkiche. "A generic battery model for the dynamic simulation of hybrid electric vehicles." 2007 IEEE vehicle power and propulsion conference. Ieee, 2007.

[38] Bazargan, Damon, Shaahin Filizadeh, and Garry Bistyak. "Battery Characterization for Vehicular Applications using hardware-in-loop real-time simulation." 2013 3rd International Conference on Electric Power and Energy Conversion Systems. IEEE, 2013.

[39] Drela, Mark. "First-order dc electric motor model." Massachusetts Institute of Technology (2007).

[40] Daud, Muhamad Zalani, Koay Zeng Kin, J. S. Norbakyah, and A. Salisa. "An optimal electric machine control system design used in plug-in hybrid electric boat." ARPN Journal of Engineering and Applied Sciences 10, no. 22 (2015): 10703-10708.

[41] Multi-Point Optimisation of a Propulsion Set as Applied to a Multi-Tasking MAV

[42] Hung, Jane Y., and Luis Felipe Gonzalez. "On parallel hybrid-electric propulsion system for unmanned aerial vehicles." Progress in Aerospace Sciences 51 (2012): 1-17.

[43] https://m-selig.ae.illinois.edu/props/volume-1/propDB-volume-1.html#APC

[44] Dehesa, Darren A., and Shyam K. Menon. "Modeling of Hybrid-Electric Powertrain for Unmanned Aerial Systems." AIAA Propulsion and Energy 2019 Forum. 2019

[45] Donateo, Teresa, Claudia Lucia De Pascalis, and Antonio Ficarella. "Synergy effects in electric and hybrid electric aircraft." Aerospace 6.3 (2019): 32.

[46] Anderson, J.D. (1999), Aircraft Performance and Design, McGraw-Hill, Boston,MA.

[47] Tian, Weiyong, Xiaohui Zhang, and Dun Yang. "Double-layer fuzzy adaptive NMPC coordinated control method of energy management and trajectory tracking for hybrid electric fixed wing UAVs." International Journal of Hydrogen Energy 47.92 (2022): 39239-39254.

[48] Dehesa Jr, Darren A. Study of control schemes for series hybrid-electric powertrain for unmanned aerial systems. Louisiana State University and Agricultural & Mechanical College, 2020.

[49] Tian, Weiyong, Xiaohui Zhang, and Dun Yang. "Double-layer fuzzy adaptive NMPC coordinated control method of energy management and trajectory tracking for hybrid electric fixed wing UAVs." International Journal of Hydrogen Energy 47.92 (2022): 39239-39254.

[50] Smith, Reid Dukes. Dynamic modeling and control of a hybrid electric quadrotor powertrain and thermal management system. Diss. University of Illinois at Urbana-Champaign, 2022.